Miner Deposita (2016) 51:639–664
DOI 10.1007/s00126-015-0627-7

ARTICLE

A refined genetic model for the Laisvall and Vassbo Mississippi Valley-type sandstone-hosted deposits, Sweden: constraints from paragenetic studies, organic geochemistry, and S, C, N, and Sr isotope data

Nicolas J. Saintilan[1,5] · **Jorge E. Spangenberg**[2] · **Elias Samankassou**[1] · **Kalin Kouzmanov**[1] · **Massimo Chiaradia**[1] · **Michael B. Stephens**[3,4] · **Lluís Fontboté**[1]

Received: 20 May 2015 / Accepted: 25 November 2015 / Published online: 22 December 2015

Abstract The current study has aimed to refine the previously proposed two-fluid mixing model for the Laisvall (sphalerite Rb-Sr age of 467 ± 5 Ma) and Vassbo Mississippi Valley-type deposits hosted in Ediacaran to Cambrian sandstone, Sweden. Premineralization cements include authigenic monazite, fluorapatite, and anatase in the Upper Sandstone at Laisvall, reflecting anoxic conditions during sandstone burial influenced by the euxinic character of the overlying carbonaceous middle Cambrian to Lower Ordovician Alum Shale Formation ($\delta^{13}C_{org}$ = −33.0 to −29.5 ‰, $\delta^{15}N_{org}$ = 1.5 to 3.3 ‰, 0.33 to 3.03 wt% C, 0.02 to 0.08 wt% N). The available porosity for epigenetic mineralization, including that produced by subsequent partial dissolution of pre-Pb-Zn sulfide calcite and barite cements, was much higher in calcite- and barite-cemented sandstone paleoaquifers (29 % by QEMSCAN mapping) than in those mainly cemented by quartz (8 %). A major change in the Laisvall plumbing system is recognized by the transition from barite cementation to Pb-Zn sulfide precipitation in sandstone. Ba-bearing, reduced, and neutral fluids had a long premineralization residence time (highly radiogenic $^{87}S/^{86}Sr$ ratios of 0.718 to 0.723) in basement structures. As a result of an early Caledonian arc-continent collision and the development of a foreland basin, fluids migrated toward the craton and expelled Ba-bearing fluids from their host structures into overlying sandstone where they deposited barite upon mixing with a sulfate pool ($\delta^{34}S_{barite}$ = 14 to 33 ‰). Subsequently, slightly acidic brines initially residing in pre-Ediacaran rift sediments in the foredeep of the early Caledonian foreland basin migrated through the same plumbing system and acquired metals on the way. The bulk of Pb-Zn mineralization formed at temperatures between 120 and 180 °C by mixing of these brines with a pool of H_2S ($\delta^{34}S$ = 24 to 29 ‰) produced via thermochemical sulfate reduction (TSR) with oxidation of hydrocarbons in sandstone. Other minor H_2S sources are identified. Upward migration and fluctuation of the hydrocarbon-water interface in sandstone below shale aquicludes and the formation of H_2S along this interface explain the shape of the orebodies that splay out like smoke from a chimney and the conspicuous alternating layers of galena and sphalerite. Intimate intergrowth of bitumen with sphalerite suggests that subordinate amounts of H_2S might have been produced by TSR during Pb-Zn mineralization. Gas chromatograms of the saturated hydrocarbon fraction from

Editorial handling: K. Kelley and G. Beaudoin

Electronic supplementary material The online version of this article (doi:10.1007/s00126-015-0627-7) contains supplementary material, which is available to authorized users.

✉ Nicolas J. Saintilan
saintila@ualberta.ca

[1] Department of Earth and Environmental Sciences, University of Geneva, Rue des Maraîchers 13, 1205 Geneva, Switzerland

[2] Institute of Earth Surface Dynamics, University of Lausanne, Building Geopolis, 1015 Lausanne, Switzerland

[3] Geological Survey of Sweden (SGU), Box 670, SE-751 28 Uppsala, Sweden

[4] Division of Geosciences, Department of Civil, Environmental and Natural Resources Engineering, Luleå University of Technology, SE-971 87 Luleå, Sweden

[5] Present address: Department of Earth and Atmospheric Sciences, University of Alberta, 1-26 Earth Sciences Building, Edmonton, AB T6G 2E3, Canada

organic-rich shale and from both mineralized and barren sandstone samples indicate that hydrocarbons migrated from source rocks in the overlying Alum Shale Formation buried in the foredeep into sandstone, where they accumulated in favorable traps in the forebulge setting.

Keywords Pb-Zn mineralization · Laisvall · Sandstone · Cambrian · Bitumen · Hydrocarbon · Alum Shale · S, C, N stable isotopes · Caledonian

Introduction

Sandstone-hosted Pb-Zn deposits are considered a subtype of Mississippi Valley-type (MVT) deposits, which are commonly hosted by carbonate rocks (cf. Leach et al. 2005). Although they are less numerous than their carbonate-hosted counterparts, important sandstone-hosted deposits include the Jinding deposit, China (200 Mt at 6.1 % Zn and 1.3 % Pb; Xue et al. 2007); the Mechernich and Maubach deposits, Germany (225 Mt at 0.3 % Zn and 1.6 % Pb, 12 Mt at 0.8 % Zn and 2.0 % Pb, respectively; Bjørlykke and Sangster 1981; Krahn and Baumann 1996); and the Laisvall deposit, Sweden (64 Mt at 4 % Pb, 0.6 % Zn, 9 g/t Ag; Årebäck and Jonsson, 2010, personal communication). The current study focuses on the Laisvall and Vassbo deposits (Sweden), which are hosted by Ediacaran to Cambrian sandstone presently located along the erosional front of the Caledonian orogen in Sweden and Norway (Fig. 1a). The world-class Laisvall deposit and the much smaller Vassbo deposit (3.2 Mt, 5.7 % Pb, 0.3 % Zn, 18 g/t Ag; Jonsson, 2010, personal communication) were mined for 60 years (1941–2001) and 22 years (1960–1982), respectively.

The aim of the current study is to present a stepwise genetic model for the Laisvall deposit in the geodynamic evolution of the western (present-day coordinates) Baltica margin during the upper Cambrian to Middle Ordovician. A multidisciplinary approach has been applied and includes mineralogical and paragenetic investigations, sulfur isotope compositions ($\delta^{34}S$) of sulfides and barite, radiogenic Sr isotope composition of pre-Pb-Zn sulfide stage barite, stable isotope composition of kerogen of potential hydrocarbon shale source rock ($\delta^{13}C_{org}$ and $\delta^{15}N_{org}$), and chemical characterization of hydrocarbons by gas chromatography-mass spectrometry in the ore, sandstone host rocks, and shale source rocks.

Our genetic model combines the results of the current work with (i) previous studies on fluid inclusion microthermometry in sphalerite and barite at Laisvall (Lindblom 1986), noble gas and halogen evidence from barite and sulfides at Laisvall and Vassbo (Kendrick et al. 2005), and earlier studies of sulfur and radiogenic lead isotope compositions of sulfides (Rickard et al. 1979, 1981; Rickard 1983; Romer 1992); (ii) the recent findings on the control of reactivated Proterozoic basement structures on the location and genesis of the Laisvall and Vassbo deposits, in particular as feeders for metal-bearing brines (Saintilan et al. 2015a); and (iii) sphalerite Rb-Sr geochronology and geochemistry indicating ore formation at Laisvall during the Middle Ordovician (467 ± 5 Ma) in a forebulge setting as a response to early Caledonian arc-continent collision and development of a foreland basin (Saintilan et al. 2015b).

Geologic setting

Caledonian orogen, autochthonous sedimentary cover rocks, and Baltica basement

In the central and northern parts of Sweden, the crystalline basement comprises Paleoproterozoic and Archean rocks belonging to a 2.0 to 1.8 Ga orogenic system (Svecokarelian orogen) and subordinate late Paleoproterozoic to early Neoproterozoic (1.7 to 0.9 Ga) sedimentary, volcanic, and intrusive rocks (Bergman et al. 2012; Fig. 1a). A thin cover of Ediacaran to Lower Ordovician sedimentary siliciclastic rocks were deposited unconformably on the crystalline basement of the western (present-day coordinates) stable platformal margin to the continent Baltica (Bergman et al. 2012; Fig. 1a). The sedimentary cover rocks are overlain in turn by thrust sheets belonging to the c. 500 to 400 Ma Caledonian orogen (Gee 1975; Roberts and Gee 1985; Bergman et al. 2012; Fig. 1a).

The Caledonian orogen resulted from a polyphase orogenic evolution (Gee 1972; Sturt 1978; Dallmeyer and Gee 1986). A foreland basin developed as a response to the collision of Baltica with an outboard island arc followed by exhumation of high-pressure rocks, including eclogites, during an early stage of the orogeny in the upper Cambrian and Lower to Middle Ordovician (Dallmeyer and Gee 1986; Santallier 1988; Stephens 1988; Kullerud et al. 1990; Gromet et al. 1996; Root and Corfu 2012). This early arc-continent collision and development of a foreland basin preceded the closure of the Iapetus Ocean and the terminal continent-continent (Laurentia-Baltica) collision, which initiated during the latest part of the Ordovician (c. 450 Ma), and continued through the Silurian and the Devonian with emplacement of the Caledonian thrust nappes (Gee 1975; Stephens 1988; Gee et al. 2010; Root and Corfu 2012; Fig. 1b).

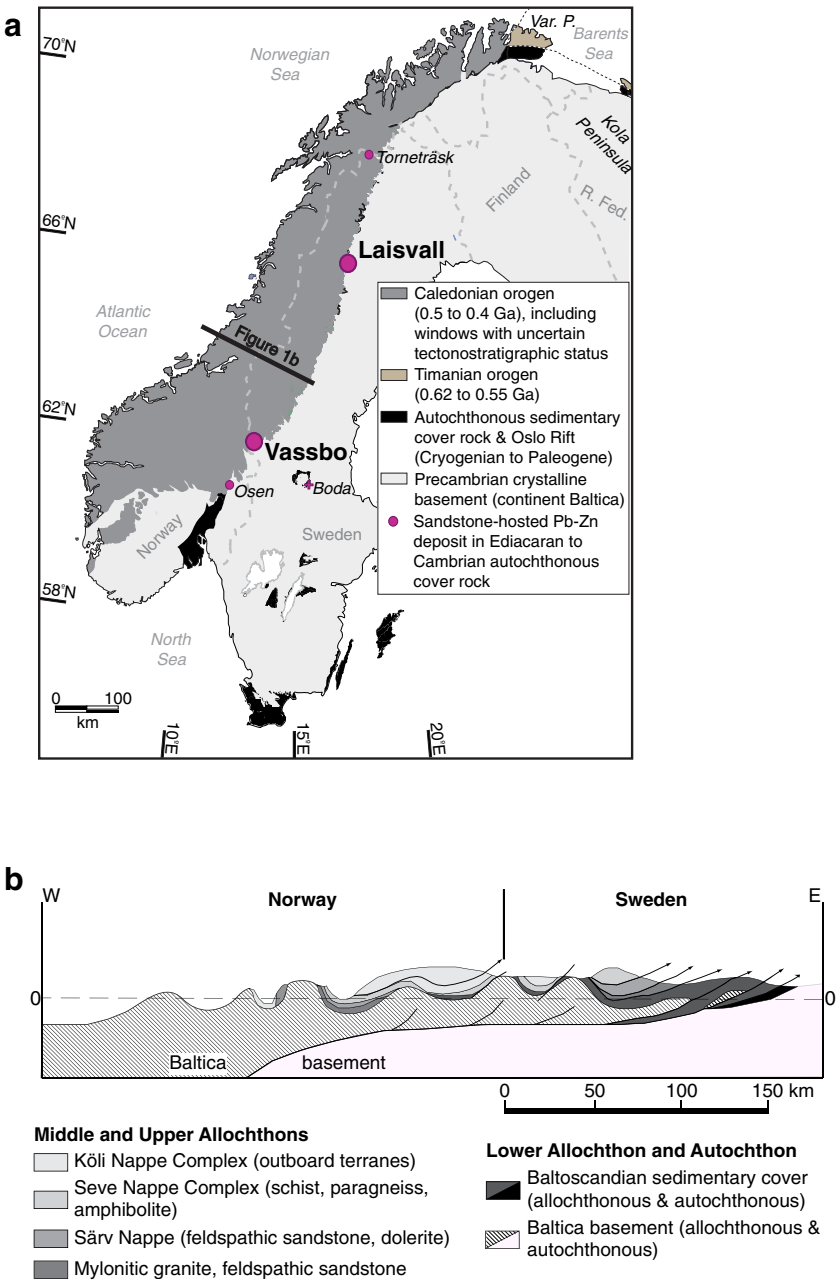

Fig. 1 **a** Simplified geologic map of Scandinavia (modified after Roberts and Siedlecka 2002; Gee et al. 2008; Bergman et al. 2012; Saintilan et al. 2015b). The locations of sandstone-hosted Pb-Zn deposits in autochthonous Ediacaran to Cambrian siliciclastic cover rocks to the crystalline basement are shown (Abbreviations: *R. Fed.* Russian Federation; *Var. P.* Varanger Peninsula). Deposits that were mined are shown as *larger dots*. The Boda Pb occurrence is hosted by Lower Ordovician limestone ~125 km SE of the erosional front of the Caledonian orogen. **b** Cross-section through the central part of the Caledonian orogen in Sweden and Norway (modified after Gee et al. 2010). *Arrows* indicate direction of thrusting

Sandstone-hosted Pb-Zn deposits in autochthonous sedimentary cover rocks

At Laisvall (Fig. 2a), the sequence of autochthonous siliciclastic rocks overlying the Paleoproterozoic (1.8 Ga) granite basement (Skiöld 1988; Bergman et al. 2012) is c. 100 m thick and is preserved underneath the main décollement to the Caledonian thrust sheets within the Alum Shale Formation. The autochthonous stratigraphy comprises the 35- to 40-m-thick Ediacaran to lower Cambrian Laisberg Formation (Willdén 1980; Nielsen and Schovsbo 2011) passing upward into the lower Cambrian Grammajukku Formation and the lowermost part of the middle Cambrian to Lower Ordovician Alum Shale Formation (Ljungner 1950; Rickard et al. 1979; Willdén 1980; Thickpenny 1984).

The Laisberg Formation (Fig. 2a) represents a transgressive, sandstone-dominated sequence (Willdén 1980; Nielsen and Schovsbo 2011). The upper part of the formation consists of a thin phosphorite pebble conglomerate in erosive contact with underlying sandstone. Epigenetic, disseminated, galena ± sphalerite mineralization is hosted in two sandstone paleoaquifers, the Lower and Upper Sandstones (Rickard et al. 1979; Willdén 1980; Saintilan et al. 2015a). Ore minerals form the cement to detrital

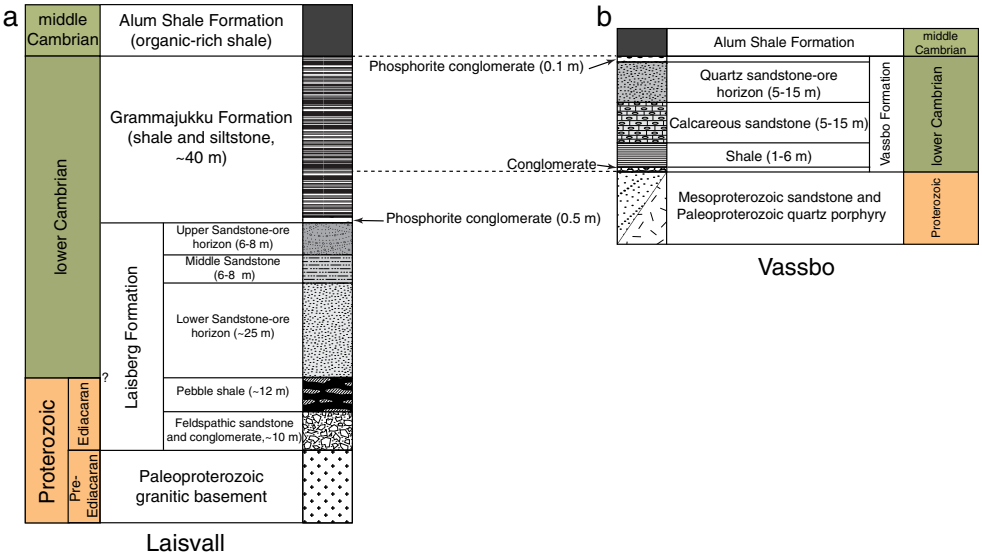

Fig. 2 **a** Stratigraphic columns of the autochthonous sedimentary cover sequence at Laisvall (modified after Rickard et al. 1979; Willdén 1980; Nielsen and Schovsbo 2011). **b** Stratigraphic column of the autochthonous sedimentary cover sequence at Vassbo (modified after Christofferson et al. 1979; Nielsen and Schovsbo 2011). Nielsen and Schovsbo (2011) proposed that the Cambrian stratigraphy at Vassbo is coeval with deposition of the Grammajukku Formation in the Laisvall area

quartz, subordinate K-feldspar (absent in the Upper Sandstone), and minor clay, monazite, zircon, apatite, and biotite (Rickard et al. 1979; Christofferson et al. 1979; Willdén 1980; Lindblom 1986; this study). In places, mineralization in the Upper Sandstone and Lower Sandstone orebodies occurs as steeply dipping galena-sphalerite-calcite veinlets (Rickard et al. 1979; Saintilan et al. 2015a).

The Laisberg Formation is capped by the local Grammajukku Formation and the regionally extensive Alum Shale Formation (Fig. 2a; Willdén 1980; Thickpenny 1984; Nielsen and Schovsbo 2011). The Grammajukku Formation comprises shale and siltstone with subordinate sandstone intercalations (Willdén 1980), whereas the Alum Shale Formation mainly consists of black- and gray-laminated, organic-rich shale (all analyzed occurrences of the Alum Shale Formation in Sweden have range of total organic carbon (TOC) content from 1 to 22 wt%; Thickpenny 1984). Deposition of ≥200 m Lower Ordovician limestone (Gee et al. 2013) contributed to sediment compaction of the Alum Shale Formation, changing its pore water regime (Israelson et al. 1996). These limestones were not preserved at Laisvall.

At Vassbo (Fig. 2b), the lower Cambrian Vassbo Formation, which is equivalent in age with the upper part of the Grammajukku Formation at Laisvall (Nielsen and Schovsbo 2011), unconformably overlies the Mesoproterozoic to Neoproterozoic basement and is capped by the partly allochthonous Alum Shale Formation (Christofferson et al. 1979; Wallin 1982; Söderlund et al. 2005; Nielsen and Schovsbo 2011). At Laisvall, Lower Ordovician limestones were not preserved at Vassbo. Galena and sphalerite mineralization is hosted in a quartz ± K-feldspar sandstone horizon in the upper part of the Vassbo Formation. Minor galena mineralization is also present in the top few centimeters of the underlying calcareous sandstone. The highest Pb and Zn grades occur at the top of sandstone paleoaquifers capped by shale aquicludes at Laisvall and Vassbo (Saintilan et al. 2015a).

Material and methods

Samples were selected from drill cores stored at the Geological Survey of Sweden (SGU) in Malå or at the Boliden Mineral core archive in Boliden (Sweden). The full workflow of sample selection and sample description is given in Electronic supplementary materials (ESM) 1. The full analytical protocols and procedures for stable (S, C, N) and radiogenic isotope (Sr) studies and for organic geochemistry studies performed on the selected samples after detailed petrographic characterizations are also given in ESM 1.

Characterization of the ore deposits and enclosing rocks

Paragenetic sequences in paleoaquifers at the Laisvall and Vassbo deposits

The relative timing of the authigenic mineral phases that formed in the Upper Sandstone and Lower Sandstone orebodies at Laisvall and the sandstone orebody at Vassbo is shown in Fig. 3 and includes data from this study and from previous works (Lindblom 1986; Lucks 2004). Three stages of porosity fill were recognized: (1) P-REE-bearing minerals such as anatase, hydrothermal monazite, and fluorapatite; (2) calcite, barite, quartz, K-feldspar, and fluorite cements; and (3) sulfides (galena, sphalerite, and pyrite; Figs. 4, 5, 6, and 7). At

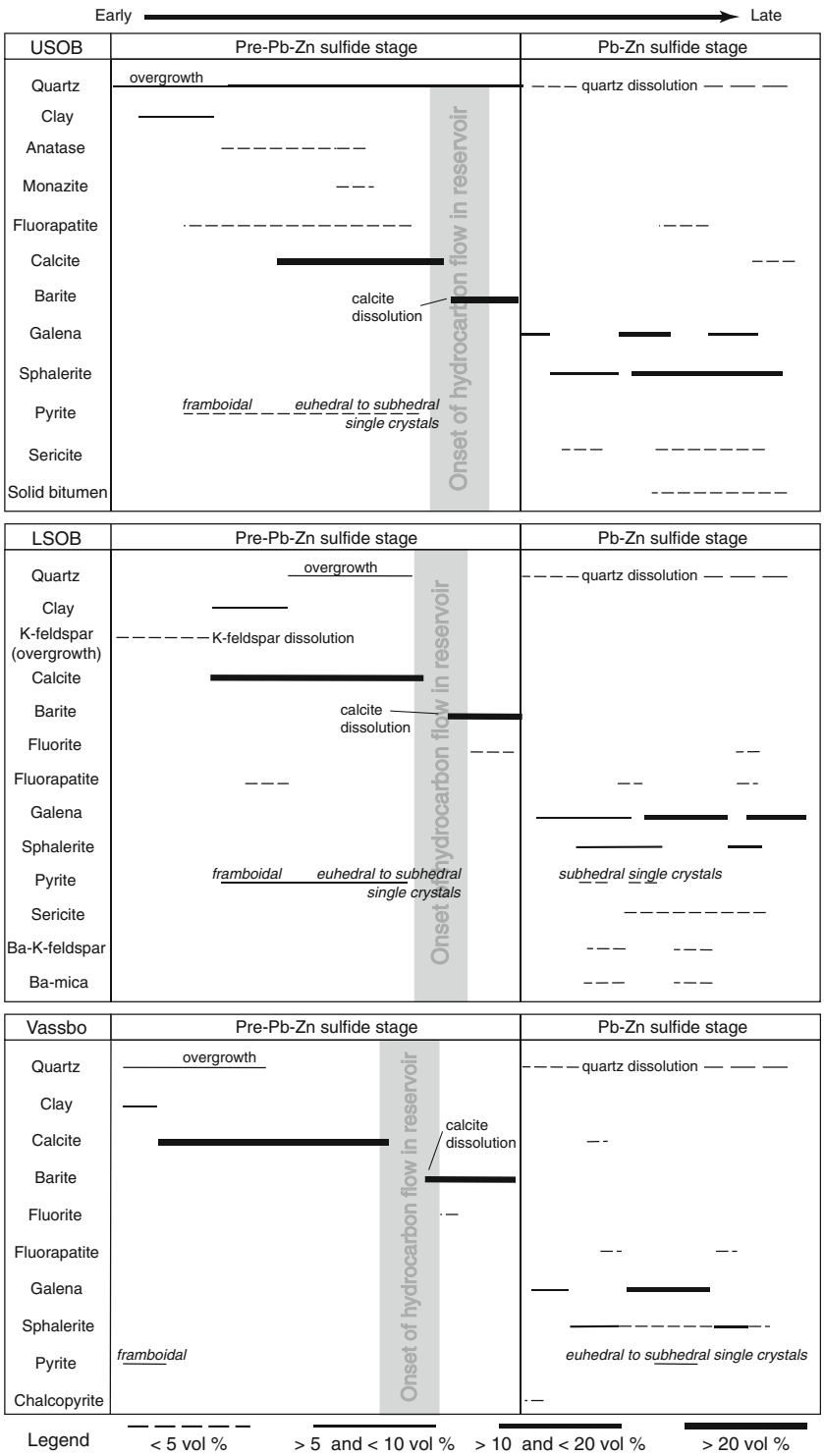

Fig. 3 Mineral assemblages and paragenetic sequences of the Upper Sandstone and Lower Sandstone orebodies (USOB and LSOB) at Laisvall and the sandstone orebody at Vassbo. Relative timing is from *left* to *right*. Monazite at Vassbo is scarce and has not been shown. It is suggested that it occupies a similar paragenetic position in the quartz sandstone at Vassbo as in the Upper Sandstone orebody at Laisvall

the two deposits, a "pre-Pb-Zn sulfide stage" and a "Pb-Zn sulfide stage" have been distinguished.

Pre-Pb-Zn sulfide stage

Quartz and calcite constitute cement in the sandstone paleoaquifers (Figs. 3, 4, and 5a–c) and both formed prior to and locally coeval with barite precipitation (Fig. 5c–e), which locally replaced calcite. QEMSCAN mapping shows that calcite is locally manganiferous. Fluorite is a minor pre-Pb-Zn sulfide stage cement (<5 vol%; Figs. 3 and 4b) in the Lower Sandstone orebody in the Central Malm area (Saintilan et al. 2015a) at Laisvall and in the sandstone orebody at Vassbo and is coeval with barite precipitation and locally replaced calcite;

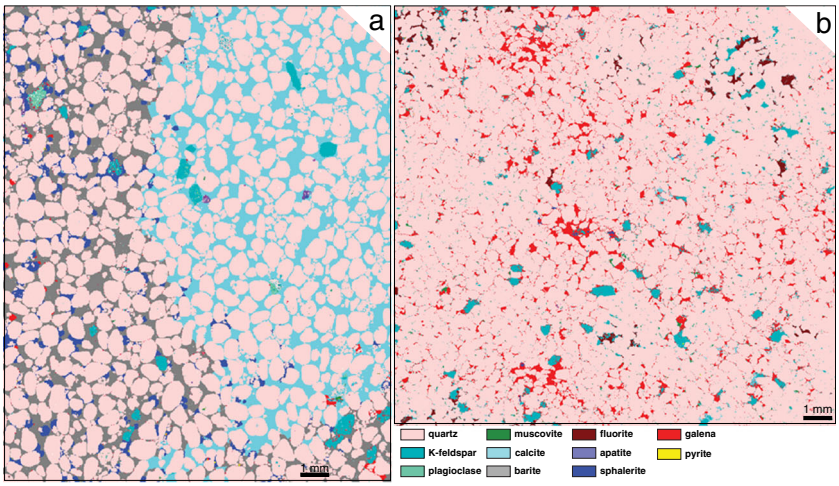

Fig. 4 **a** QEMSCAN image of the sandstone orebody at Vassbo. **b** QEMSCAN image of a quartz-galena-fluorite ± barite ± calcite cemented part of the Lower Sandstone at Laisvall

fluorite is scarce in the Upper Sandstone orebody. Pyrite is commonly framboidal and occurs also as aggregates of euhedral pyrite.

In the Upper Sandstone orebody, anatase and hydrothermal monazite form a P-REE-Ti mineral assemblage associated with quartz overgrowths and pyrite. Anatase typically coats detrital quartz, detrital zircon, and detrital monazite and is locally included in quartz overgrowths (Fig. 6a). Hydrothermal monazite ranges in size from 220 to 450 μm and may constitute up to 0.01 vol% of the sandstone. It is locally embedded in a clay matrix, is intergrown with pyrite, and coats quartz overgrowths around detrital quartz (Fig. 6b).

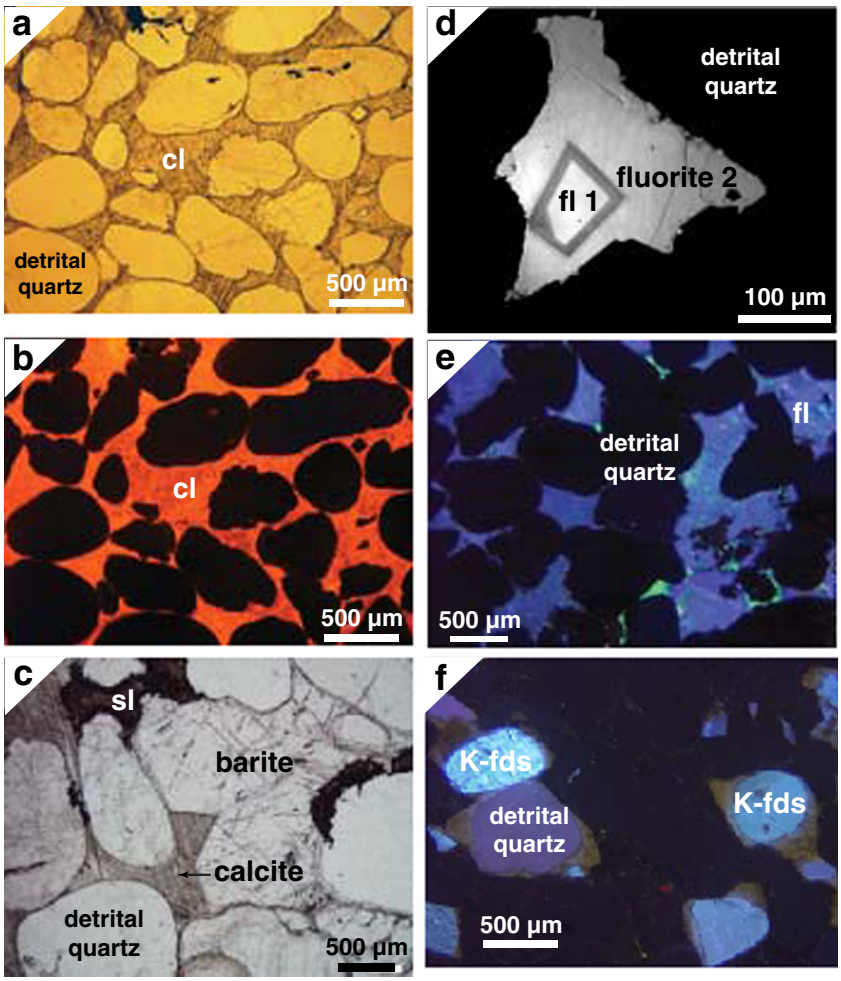

Fig. 5 **a** Pre-Pb-Zn sulfide stage calcite (*cl*) cement in the sandstone orebody at Vassbo (transmitted light). **b** Same field observation as in **a**: optical cathodoluminescence image of the calcite cement. **c** Pre-Pb-Zn sulfide stage calcite and subsequent barite cements in the sandstone orebody at Vassbo (transmitted light). Sphalerite precipitated after reductive dissolution of barite. **d** Fluorite cement in the Lower Sandstone at Laisvall (scanning electron microprobe image in cathodoluminescence mode, SEM-CL). There is evidence for two generations of fluorite growth: (1) euhedral fluorite (*fl*) suggestive of relatively stable hydrodynamic conditions, (2) anhedral fluorite with complex crystallinity. **e** Optical cathodoluminescence image of a fluorite-cemented zone (*blue-green tints*) of the Lower Sandstone at Laisvall. **f** Detrital K-feldspar and Ba-bearing overgrowths (*yellowish tint*) in the Lower Sandstone at Laisvall

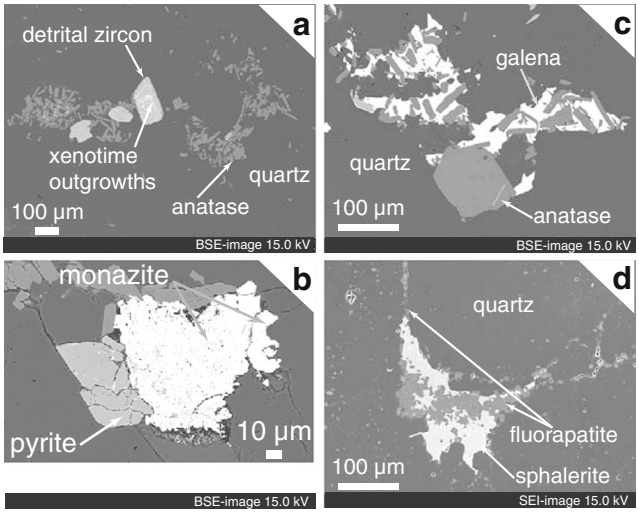

Fig. 6 **a** Quartz-cemented Upper Sandstone at Laisvall with authigenic anatase coating detrital quartz, zircon, and monazite. Xenotime forms outgrowths on detrital zircons (backscattered electron, BSE). **b** Authigenic monazite associated with subhedral nonframboidal pyrite. The largest monazite grain has multiple nanoscale galena inclusions that are probably related to U decay in monazite. The smallest monazite grain does not show any inclusions (SEM-BSE image). **c** Authigenic anatase coating quartz. Anatase was cemented by galena (BSE image). **d** Authigenic fluorapatite coating detrital quartz and included in quartz overgrowths. A second generation of aggregates of euhedral to subhedral fluorapatite, co-genetic with sphalerite, has been identified (secondary electron mode, SEI)

Minor galena (<0.1 vol%) is present between anatase grains (Fig. 6c) but also in anhedral hydrothermal monazite grains; U decay from monazite grains may have contributed Pb for galena precipitation (Fig. 6b). Xenotime outgrowths on zircon were observed locally (Fig. 6a). Fluorapatite, identified by scanning electron miscroscopy coupled with energy dispersive X-ray spectroscopy (SEM-EDX) analyses, is typically in the range of 50 to 450 µm and constitutes about 0.02 vol %. Fluorapatite coats detrital quartz and is commonly included in quartz overgrowths (Fig. 6d).

The Lower Sandstone orebody lacks this peculiar P-REE-Ti mineral association. Only scarce fluorapatite was observed. The Lower Sandstone orebody is the only paleoaquifer characterized by extensive Ba-bearing K-feldspar overgrowth/cement around detrital K-feldspar grains (Lucks, 2004; this study). Optical cathodoluminescence images show a systematic yellowish tint of the Ba-bearing overgrowths around the detrital K-feldspar grains, which are characterized by different tints (e.g., light blue, pink) of cathodoluminescence indicative of a heterogeneous provenance (Fig. 5f).

The sandstone orebody at Vassbo shares most of the characteristics of the Lower Sandstone orebody at Laisvall. Exceptions include the occurrence of fluorapatite, which can constitute up to 0.5 vol% in some samples, and locally hydrothermal monazite, ranging in size from 110 to 140 µm (<0.01 vol%), similar to that observed in the Upper Sandstone orebody at Laisvall.

Based on QEMSCAN mapping data (ESM 2) and mineral texture relationships, mineral phases were classified into two groups as explained below: (i) detrital phases (e.g., quartz, K-feldspar, zircon, mica), quartz ± K-feldspar cements, framboidal and euhedral to subhedral pyrite; and (ii) calcite, barite ± fluorite, and Pb-Zn sulfides. For each group, the total sum of pixels occupied by each mineral phase was calculated and divided by the total amount of pixels in the image. In this manner, an estimate was made for the fraction of porosity occupied by calcite and barite cements. These cements protected sandstone from quartz cementation and, unlike quartz, were prone to dissolution and replacement at a later stage by sulfides. QEMSCAN mapping show that this porosity may be as much as 29 vol% (Fig. 4a). By contrast, in sandstone dominated by quartz cement (Fig. 4b), the porosity occupied by Pb-Zn sulfides ± calcite ± barite ± fluorite cements is only about 8 vol%.

Pb-Zn sulfide ore stage

Pb and Zn sulfides are interstitial to detrital quartz grains. Thin sections of representative ore samples from the Upper Sandstone and Lower Sandstone orebodies at Laisvall are shown in Fig. 7a. The Upper Sandstone orebody is characterized by alternating layers of galena and yellow-orange sphalerite with local clusters of sphalerite or galena. Galena in the Lower Sandstone orebody typically forms large clusters (up to several millimeters across) which in places form continuous layers roughly parallel to bedding. Honey to light beige sphalerite also occurs as clusters. Mineralization in the sandstone orebody at Vassbo is similar to that in the Lower Sandstone orebody at Laisvall. In both the Laisvall and Vassbo orebodies, the contacts between quartz and Pb-Zn sulfides are irregular. Lead-zinc sulfides are coeval with and/or postdate local quartz dissolution indicated by serrated edges (Fig. 7b, c). Both detrital quartz and diagenetic quartz overgrowths were affected by this episode of dissolution (Fig. 7b).

In detail, galena and sphalerite show complex intergrowths that represent repeated episodes of precipitation and replacement (Fig. 3). Sphalerite, particularly that in the Upper Sandstone orebody at Laisvall but also at Vassbo, is typically intergrown with euhedral to subhedral, 10- to 30-µm-large fluorapatite crystals (Figs. 6d and 7b). Galena is commonly intergrown with <20-µm-long Ba-K-feldspar and Ba-mica in the Lower Sandstone orebody at Laisvall and in the sandstone orebody at Vassbo (Fig. 7c). Furthermore, sericite shards are commonly intergrown with Pb-Zn sulfides (Fig. 7d, e). Chalcopyrite ($\ll 1$ vol %) is rare.

Ore-stage calcite is not abundant in the orebodies at Laisvall and Vassbo. It occurs in small amounts, in the Upper Sandstone orebody and in the sandstone orebody at Vassbo (Fig. 7f, g), but was not identified in the Lower Sandstone orebody. Ore-stage calcite grains are

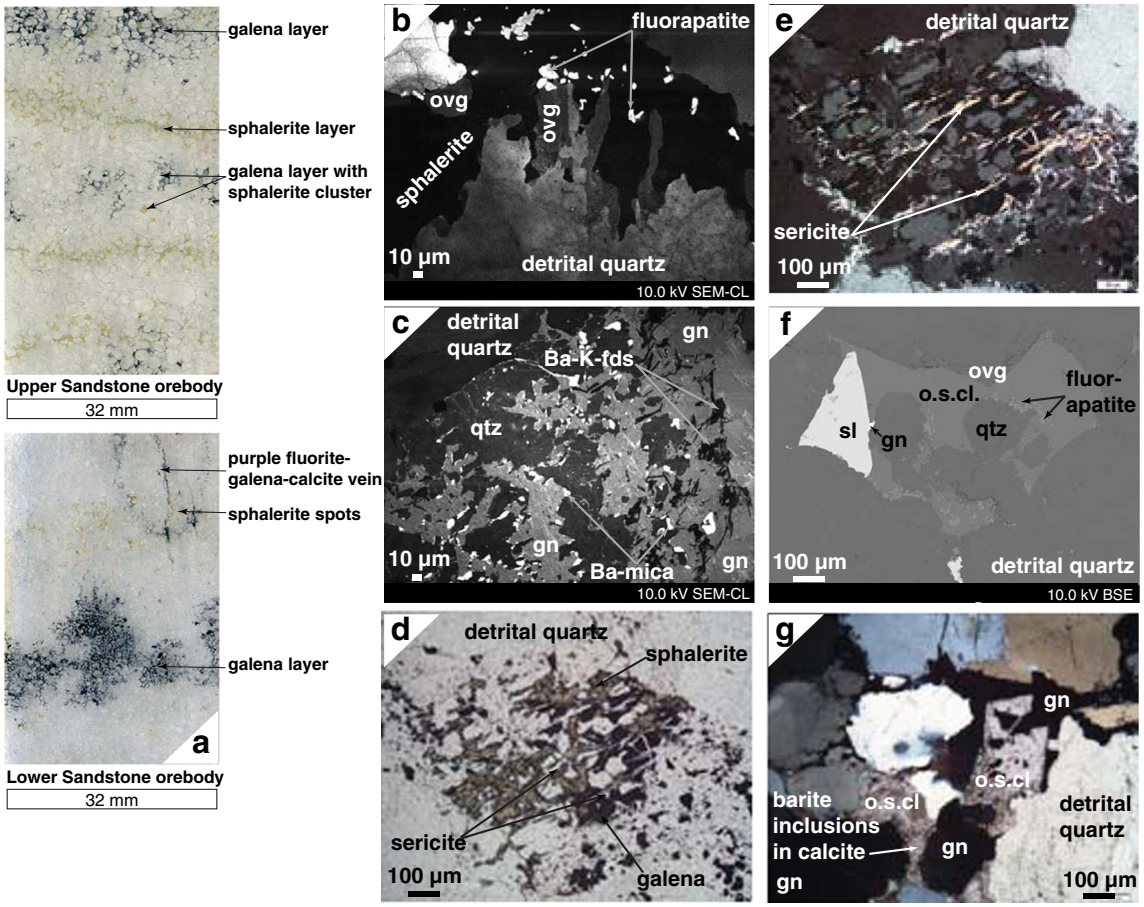

Fig. 7 **a** Representative thin sections of Pb-Zn mineralization in the Upper Sandstone and Lower Sandstone orebodies at Laisvall. The Upper Sandstone orebody typically shows alternating bands of galena and sphalerite, whereas the Lower Sandstone orebody is characterized by galena and sphalerite clusters and, only locally, galena bands. **b** SEM-CL image of sphalerite ± fluorapatite mineralization interstitial to detrital quartz with diagenetic overgrowths showing serrated edges suggesting etching (Upper Sandstone orebody, Laisvall). **c** SEM-CL image of galena ± Ba-K-feldspar ± Ba-mica mineralization between detrital quartz with diagenetic overgrowths showing dissolution features (Lower Sandstone orebody, Laisvall). **d** Details of sphalerite-galena mineralization intergrown with sericite and ore-stage quartz in the Lower Sandstone orebody, Laisvall (transmitted light). **e** Same field of observation as in **d** (transmitted light, crossed nicols). **f** SEM-BSE image of ore-stage calcite (*o.s.cl.*) and sphalerite ± galena after quartz overgrowth and fluorapatite precipitation (Upper Sandstone orebody, Laisvall). **g** Galena associated with anhedral to subhedral ore-stage calcite after reductive dissolution of barite in the Upper Sandstone orebody, Laisvall (transmitted light, crossed nicols)

less than 100 μm and fill in the porosity left between quartz and fluorapatite. Subhedral ore-stage calcite (<100 μm) intergrown with galena is common where galena replaced barite cement in the Upper Sandstone orebody (Fig. 7g).

Solid bitumen in the cementing phases

Locally, in the Lower Sandstone orebody at Laisvall, premineralization barite ± calcite ± fluorite cement contains abundant black solid aggregates, particularly as inclusions in barite. They are mostly present in barren parts or in spots where Pb-Zn sulfides precipitated after dissolution of both barite and quartz. These black solid inclusions were identified as bitumen by SEM-backscattered electron (BSE) images and SEM-EDX analysis. Raman spectrometry of these inclusions shows main peaks at 1324–1327 and 1607 cm^{-1}, similar to those in spectra obtained for solid bitumen from the San Vicente Zn-Pb MVT deposit, Peru (Spangenberg and Macko 1998). Solid bitumen in the Upper Sandstone orebody is commonly intergrown with sphalerite (Fig. 8a), in particular where sphalerite forms relatively continuous layers (Fig. 7a). The characteristic Raman peak of CH_4 at 2913 cm^{-1} was recognized in black fluid inclusions in this sphalerite species. These observations are consistent with previous results that suggested that the mineralizing fluids contained "petroleum-like compounds" (Rickard et al. 1975) and the optically recognized hydrocarbons in fluid inclusions (Lindblom 1986). The section below on the molecular composition of bitumens constrains the type and origin of these "petroleum-like compounds."

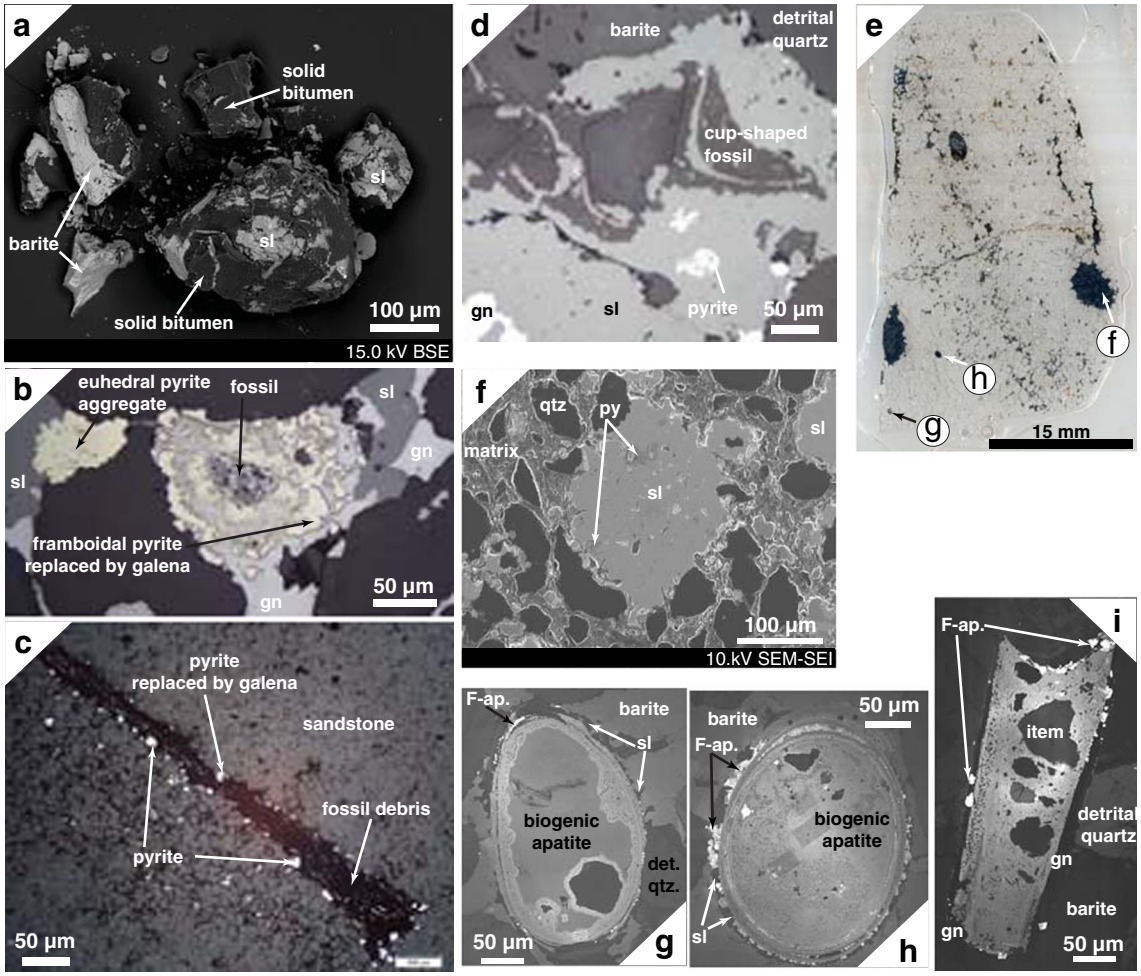

Fig. 8 **a** Fragments picked from the 315- to 125-µm size fraction mounted on a stub and covered with gold showing solid bitumen intergrowth with sphalerite (*sl*) and solid bitumen inclusions in barite (SEM-BSE image). **b** Reflected light microscopy image showing fossil in an aggregate of framboidal pyrite replaced by galena (*gn*) and sphalerite. Euhedral pyrite aggregates are also replaced by sphalerite. **c** Irregular framboidal pyrite replaced by galena and/or sphalerite in fossil lamellae or tubes (reflected light). **d** Cup-shaped fossil debris where framboidal pyrite was replaced by sphalerite ± galena. **e** Scan of representative thin section of the barite-calcite-galena-sphalerite-cemented sandstone orebody at Vassbo. Black pebbles several millimeters in diameter and several dark-green to black ovoid pellets (<1–2 mm) are disseminated in the sandstone. **f** Detail of one of the black pebbles that are composed of quartz fragments and 100–200 µm sulfide aggregates in clay-phyllosilicate matrix (SEM-SEI image). **g**, **h** SEM-CL images of dark-green to black ovoid fecal pellets consisting of biogenic apatite and various inclusions of unknown minerals. Sphalerite was precipitated at the interface between the fecal pellets and matrix after reductive dissolution of barite cement. **i** Angular porous fragment of biogenic apatite with inclusions of crystal fragments. This fragment has a reaction rim of galena and fluorapatite at the interface with barite cement (SEM-CL image)

Organic debris in the sandstone orebodies at Vassbo and Laisvall

In the sandstone orebody at Vassbo, in particular where microfossils and other organic debris are abundant, framboidal pyrite is commonly replaced by Pb-Zn sulfides. Typically, microfossils (<50 µm) are enclosed in pyrite aggregates that are replaced by galena and/or sphalerite (Fig. 8b). Framboidal pyrite replaced by galena and/or sphalerite is also found in fossil lamellae or tubes (Fig. 8c) and cup-shaped fossil debris (Fig. 8d), which resemble pyritized organic clots identified as algal fragments in Cambrian black-shale-hosted polymetallic Ni-Mo deposits in South China (Cao et al. 2013).

Figure 8e shows barite-calcite-galena-sphalerite-cemented sandstone at Vassbo, with black pebbles several millimeters across (Fig. 8e, f). These black pebbles are composed of quartz fragments and 100- to 200-µm-large sulfide aggregates embedded in clay-phyllosilicate matrix. SEM images (secondary electron, SEI, and cathodoluminescence, SEM-CL, modes) reveal that preexisting pyrite aggregates were replaced by sphalerite (Fig. 8f).

In addition, dark-green to black ovoid pellets (<1 to 2 mm) are disseminated in the sandstone at Vassbo (Fig. 8e, g, h). These pellets consist of apatite and various occluded components (mostly quartz fragments). By analogy with pellets described elsewhere, we propose that these features are fecal

pellets made of biogenic apatite. Similar phosphatized fecal pellets are reported from various deposits in South China in formations contemporaneous with the lower Cambrian Vassbo Formation (in the lower Cambrian Xiaoton section and in the lower Cambrian part of the Niutitang Formation; Kribek et al. 2007; Cremonese et al. 2013; Shields-Zhou and Zhu 2013; Shen et al. 2014). Fecal pellets commonly found in recent analogs, e.g., Cretaceous Negev phosphorites, Israel (Soudry and Champetier 1983), and Paleocene to Eocene phosphorite sedimentary deposit at Ras-Draâ, Tunisia (Ben Hassen et al. 2010), are remarkably similar to the pellets identified in sandstone at Vassbo. Sphalerite and fluorapatite precipitated on the rims of these fecal pellets after dissolution of the surrounding barite cement (Fig. 8g, h).

At Laisvall, framboidal pyrite and organic debris are less abundant. However, angular fragments of biogenic apatite with a porous texture and including various types of debris were identified (Fig. 8i). Similar reaction rims of galena and fluorapatite are present at the contact between fossils and barite cement.

Sulfur isotope composition of sulfides and barite

The range and distribution of $\delta^{34}S$ values of the analyzed sulfide and sulfate minerals in the orebodies at Laisvall and Vassbo are graphically presented in Fig. 9 and summarized statistically in Table 1. The data are given in ESM 3. These data were combined with previous data from Laisvall (Rickard et al. 1979; Rickard et al. 1981) and Vassbo (Wallin 1982; Broman 1983).

The $\delta^{34}S$ values of sphalerite and galena from disseminated mineralization at Laisvall and Vassbo are all positive, ranging between 14.2 and 34.1 ‰ and 11.5 and 29.2 ‰, respectively. Sphalerite and galena with relatively light values (<21.4 and <17.5 ‰, respectively) are from the Vassbo deposit. Compared to Pb-Zn sulfides at Laisvall, the distribution of sphalerite $\delta^{34}S$ values at Vassbo is bimodal: one mode at 19.5 ± 2.1 ‰ (1 standard deviation, $n = 10$) and the other at 32.9 ± 1.2 ‰ ($n = 2$).

At Laisvall, the sphalerite $\delta^{34}S$ values in the Upper and Lower Sandstones show similar ranges (21.4 to 33.8 ‰ and 24.1 to 31.5 ‰, respectively) with average values of 29.2 ± 2.5 ‰ ($n = 22$) and 28.6 ± 2.1 ‰ ($n = 18$), respectively. The $\delta^{34}S$ values for galena in the Upper and Lower Sandstones (18.3 to 28.8 ‰ and 17.5 to 29.2 ‰, respectively) are also remarkably similar with average values of 24.2 ± 2.7 ‰ ($n = 33$) and 23.7 ± 3.4 ‰ ($n = 40$), respectively. By contrast, sphalerite in the Upper Sandstone orebody in the feeder fault area of the Central Malm at Laisvall (Saintilan et al. 2015a) has a value of 2.3 ‰. Galena in steeply dipping veinlets in the Upper and Lower Sandstones also has positive values, overlapping with those from disseminated galena mineralization.

At Laisvall, barite in the Upper Sandstone orebody has values between 14.2 and 32.7 ‰ (21.8 ± 5.9 ‰, $n = 8$), whereas barite in the Lower Sandstone samples averages 5 ‰ lighter (15.1 ± 0.8 ‰, $n = 2$). $\delta^{34}S$ values of barite in the sandstone orebody at Vassbo are similar to those at Laisvall, ranging between 16.2 and 23.1 ‰.

Euhedral pyrite in the Upper and Lower Sandstones at Laisvall has $\delta^{34}S$ values between 21.0 and 32.5 ‰ (26.0 ‰, $n = 20$). The values of euhedral to subhedral pyrite at Vassbo range from 9.3 to 17.7 ‰ (15.3 ± 2.5 ‰, $n = 10$) with some higher values at 24.4 and 28.7 ‰ (26.5 ± 2.1 ‰, $n = 2$).

By contrast, framboidal pyrite of the Grammajukku Formation has a $\delta^{34}S$ value of −10.1 ‰. Furthermore, one sample of pyrite in the Upper Sandstone orebody at Laisvall, at the contact with the overlying shale of the Grammajukku Formation (Fig. 2a) has a $\delta^{34}S$ value of −6.4 ‰. At Vassbo, a framboidal pyrite sample has a $\delta^{34}S$ value of −8.0 ‰, whereas $\delta^{34}S$ values for pyrite in the phosphorite conglomerate above the sandstone orebody (Fig. 2b) range between −13.1 and 7.5 ‰.

Above the Vassbo deposit, pyrite in organic-rich shale of the Alum Shale Formation has $\delta^{34}S$ values between 6.8 and 7.6 ‰. These values are lower than the values for pyrite in the Alum Shale Formation at Laisvall (14.5 to 16.0 ‰; Rickard et al. 1979). The difference in the sulfur isotope composition of pyrite between the two locations of Alum Shale Formation is discussed in later sections.

Strontium isotope composition of barite and phosphorite

Barite in the Upper Sandstone and Lower Sandstone orebodies at Laisvall has $^{87}Sr/^{86}Sr$ ratios of 0.718791 ± 14 and 0.722349 ± 14, respectively (Table 2). The phosphorite pellet aliquot from the phosphorite conglomerate has a $^{87}Sr/^{86}Sr$ ratio of 0.721016 ± 14.

Total organic carbon and nitrogen contents and carbon and nitrogen isotope composition of organic matter in shale at Laisvall

The dark gray and black shale samples of the Alum Shale Formation have TOC and total organic nitrogen (TON) contents of 0.33 to 3.03 wt% (average value of 1.27 ± 0.94 wt%, $n = 12$) and 0.02 to 0.08 wt% (0.06 ± 0.02 wt%, $n = 8$), respectively (Table 3). The $\delta^{13}C_{org}$ values vary from −32.5 to −29.5 ‰ (−31.2 ± 1.4 ‰, $n = 12$) and the $\delta^{15}N_{org}$ values from 1.5 to 3.3 ‰ (2.3 ± 0.7 ‰, $n = 8$).

The green and gray shale samples of the Grammajukku Formation have TOC and TON contents of 0.12 to 0.20 wt % (0.16 ± 0.02 wt%, $n = 8$) and 0.03 to 0.07 wt% (0.05 ± 0.01 wt%, $n = 12$), respectively (Table 3). The $\delta^{13}C_{org}$ values

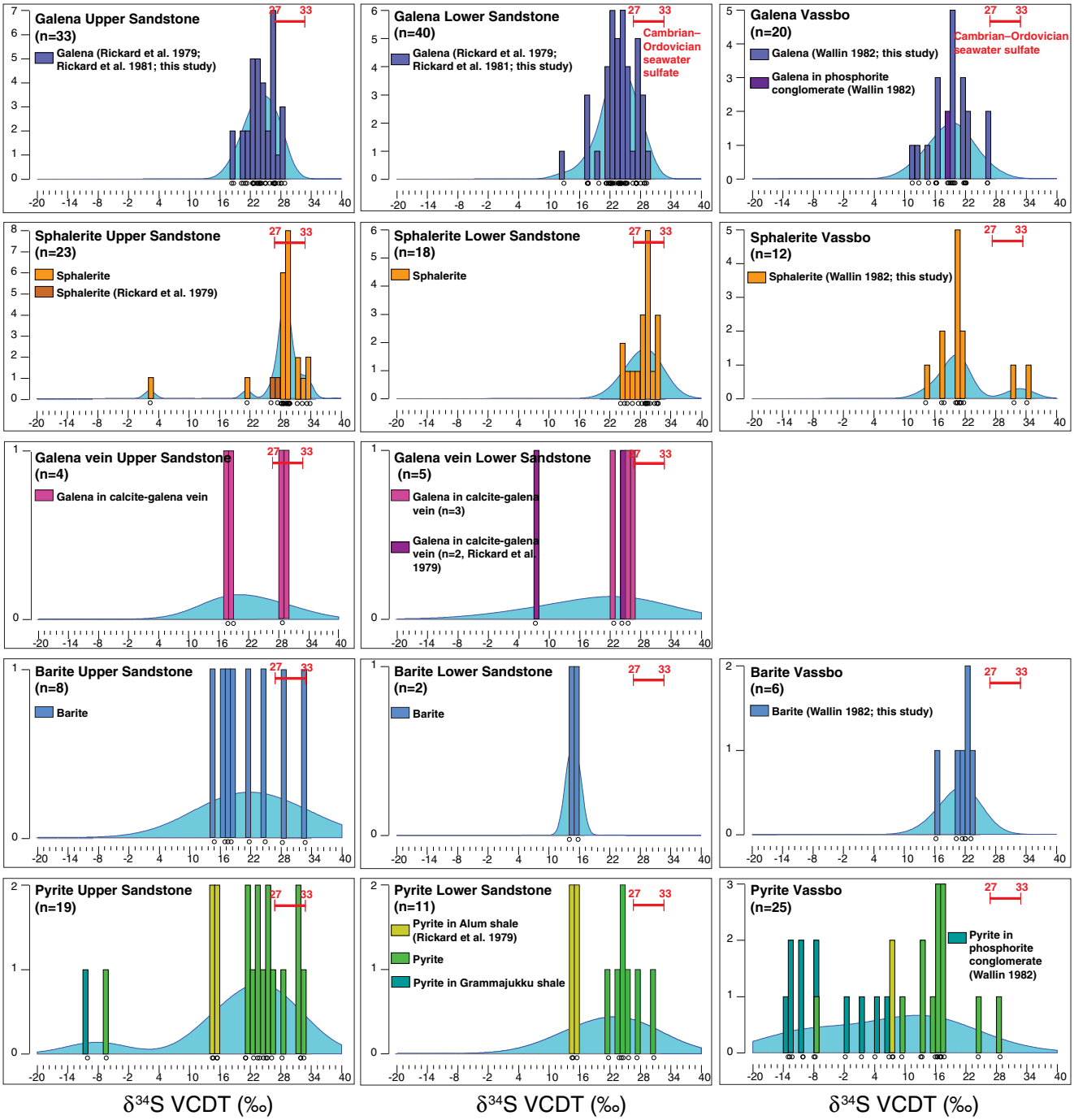

Fig. 9 Frequency distribution diagrams of $\delta^{34}S$ values for galena, sphalerite, galena in veinlets, barite, and pyrite in the Upper Sandstone and Lower Sandstone orebodies at Laisvall compared to those in the sandstone orebody at Vassbo. The background *blue curves* are kernel frequency distribution curves identifying one or several populations of $\delta^{34}S$ values for each mineral in each orebody

vary from −32.3 to −29.2 ‰ (−30.4 ± 1.0 ‰, $n = 8$) and the $\delta^{15}N_{org}$ values from 2.1 to 3.3 ‰ (2.8 ± 0.4 ‰, $n = 12$).

The two types of shale formation have similar $\delta^{13}C_{org}$ and $\delta^{15}N_{org}$ values and TON contents despite the much lower TOC contents of the shales in the Grammajukku Formation in comparison to those of the shales in the overlying Alum Shale Formation.

Molecular composition of bitumens

Representative gas chromatograms (GC) of the saturated hydrocarbon (HC) fraction from the organic-rich (TOC 1.08 wt %) shale samples ASF4-1 and ASF4-2, the mineralized Upper Sandstone and Lower Sandstone samples, and the barren Lower Sandstone sample are shown in Fig. 10. The dominant

Table 1 Sulfur isotope data of sulfides and sulfates from the orebodies at the Laisvall and Vassbo deposits

Mineral	δ^{34}S (‰, VCDT) range (average ± 1 standard deviation, number of samples[a] = *x*)
Upper Sandstone orebody, Laisvall	
Sphalerite[b]	21.4–33.8 (29.2 ± 2.5, 22)
Galena	18.3–28.8 (24.5 ± 2.7, 33)
Galena in vein	17.8–28.4 (23.5 ± 5.1, 4)
Pyrite (nonframboidal)	21.0–32.5 (26.0 ± 5.9, 13)
Barite	14.2–32.7 (21.8 ± 5.9, 8)
Lower Sandstone orebody, Laisvall	
Sphalerite	24.1–31.5 (28.6 ± 2.1, 18)
Galena	17.5–29.2 (23.7 ± 3.4, 40)
Galena in vein	22.7–26.1 (24.6 ± 1.3, 5)
Pyrite (nonframboidal)	21.7–30.6 (25.4 ± 2.6, 7)
Barite	14.0–15.7 (15.1 ± 0.8, 2)
Quartz sandstone orebody, Vassbo	
Sphalerite	14.2–21.7 (19.5 ± 2.2, 10) and 31.6–34.1 (32.9 ± 1.2, 2)
Galena	11.5–26.3 (19.2 ± 3.8, 18)
Pyrite (nonframboidal)	9.3–17.7 (15.3 ± 2.5, 11) and 24.4–28.7 (26.5 ± 2.1, 2)
Barite	16.2–23.1 (20.8 ± 2.2, 6)

[a] This study, Rickard et al. (1979, 1981), and Wallin (1982)

[b] Except sphalerite in the feeder fault area of the Central Malm ($n = 1$) with sulfur isotope composition of 2.3 ‰

resolvable compounds in the GC traces of the saturated HC are *n*-alkanes in the C_{15}–C_{32} range with maxima between C_{19} and C_{23}, pristane (Pr), and phytane (Ph). Bell-shaped features corresponding to high amounts of unresolved complex mixture (UCM) of hydrocarbons eluting between C_{17} and C_{28} are present and characteristic of the GC traces of the organic-rich shale and the mineralized sandstone samples (Fig. 10a–c). Bacterial degradation and oxidative degradation by hydrothermal fluids, which may have induced some water washing, can explain the broad hump in the UCM. Furthermore, radiolytic damage identified as a possible process yielded broad humps of UCMs (e.g., Witwatersrand bitumen, South Africa, Spangenberg and Frimmel 2001; Pribram deposit, Czech Republic, Kribek et al. 1999). In the case of U-rich alum shales (Thickpenny 1984), radiolytic damage of hydrocarbons cannot be excluded as an additional process for this hump in the UCM.

Table 2 Strontium isotope data for phosphorite pellets in the conglomerate above the Upper Sandstone and barite cement in the Upper and Lower Sandstones (Laisberg Formation, Laisvall)

Sample	Stratigraphy at Laisvall	$^{87}Sr/^{86}Sr$	$\pm 2\sigma$ ($\times 10^{-6}$)
11LAI16-1	Phosphorite pellet in phosphorite polymict conglomerate	0.721016	14
12LAI73	Barite cement in Upper Sandstone ore horizon	0.718791	14
12LAI64	Barite cement in Lower Sandstone ore horizon	0.722349	14

The distribution of *n*-alkanes does not show any odd over even C-predominance (CPI = 0.93–1.04; Table 4), except for the barren sandstone sample (Fig. 10d), which is characterized by a dominance of even C homologues (CPI = 0.55). The distribution of hopanes (*m*/*z* 191) and steranes (*m*/*z* 217) in the organic-rich shale and mineralized sandstone samples is remarkably similar (Fig. 11). Tricyclic triterpanes in the range C_{25}–C_{29} and hopanes in the range C_{27}–C_{35} were identified in the *m*/*z* 191 mass chromatograms of all samples. Steranes in the C_{27}–C_{29} range were detected in the *m*/*z* 217 mass chromatograms of the analyzed samples.

The difference between the barren and mineralized samples (Fig. 10; Table 4) can be summarized as follows: (i) the presence of a UCM is characteristic of the GCs of the mineralized sandstone samples and Alum Shale samples; (ii) the maxima in the *n*-alkanes distribution are in the $C_{22–23}$ range in the mineralized samples and at C_{20} in the barren one; (iii) the Ph/*n*-C_{18} ratios are higher in the mineralized samples; and (iv) low molecular weight hydrocarbons with carbon number lower than C_{22}, which are commonly considered as marine algal and/or bacterial derivatives (cf. Gelpi et al. 1970; Spangenberg and Herlec 2006), are common to and characteristic of the mineralized sandstone and Alum Shale samples.

These results are consistent with the results of a study that identified the kerogen structure of the Alum Shale Formation as primarily consisting of algal organic matter (Bharati et al. 1995). More importantly, the hydrocarbon distributions and biomarkers indicate a common algal and bacterial source of organic matter for the derivatives found in the Alum Shale Formation and the mineralized sandstone samples.

Interpretation of the petrographic and analytical data

Pre-Pb-Zn sulfide stage in sandstone

New insights into the depositional environment of the Alum Shale Formation

The low $\delta^{13}C_{org}$ values (average values of −31.2 and −30.4 ‰, respectively) in the middle Cambrian to Lower Ordovician Alum Shale and lower Cambrian Grammajukku Formations suggest an isotopically light carbon source with consumption of ^{13}C-depleted inorganic carbon (DIC) derived from oxidation of dissolved organic carbon (DOC) compounds. In addition, the ranges of $\delta^{15}N_{org}$ values and nitrogen contents in the Alum Shale Formation (1.5 to 3.3 ‰ and 0.02 to 0.08 wt% N, respectively) are in accordance with N_2 fixation as the

Table 3 Total organic carbon content (TOC wt% C), carbon isotope data, total nitrogen content (TON wt% N) and nitrogen isotope data of organic matter in shale samples from the Alum Shale and Grammajukku Formations in the stratigraphy at Laisvall

Samples		TOC (wt% C) range (average ± 1 standard deviation, $n = x$)	$\delta^{13}C_{org}$ (‰ VPDB) range (average ± 1 standard deviation, $n = x$)	TON (wt% N) range (average ± 1 standard deviation, $n = x$)	$\delta^{15}N_{org}$ (‰ AIR-N2) range (average ± 1 standard deviation, $n = x$)
ASF11	Black shale above limestone horizon, Alum Shale Formation	2.65–3.03 (2.80 ± 0.17, 3)	−32.5 to −32.0 (−32.3 ± 0.2, 3)	0.08	2.0–2.1 (2.0 ± 0.1, 2)
ASF9	Dark gray shale, Alum Shale Formation	1.14–1.35 (1.24 ± 0.09, 3)	−33.0 to −32.8 (−32.9 ± 0.1, 3)	0.08	1.5–1.6 (1.5 ± 0.1, 2)
ASF10	Dark gray shale, Alum Shale Formation	0.55–0.84 (0.66 ± 0.13, 3)	−29.8 to −29.5 (−29.6 ± 0.1, 3)	0.05	2.2 (2.2 ± 0.0, 2)
ASF4-0	Dark gray shale, Alum Shale Formation	0.33–0.41 (0.38 ± 0.03, 3)	−30.8 to −29.5 (−30.1 ± 0.5, 3)	0.02–0.03	3.3 (3.3 ± 0.0, 2)
		1.27 ± 0.94 ($n = 12$)	−31.2 ± 1.4 ($n = 12$)	0.06 ± 0.02 ($n = 8$)	2.3 ± 0.7 ($n = 8$)
ASF1	Green-gray shale, Grammajukku Formation	0.17 (1)	−32.3 (1)	0.06	2.7 (2.7 ± 0.0, 2)
ASF7	Gray shale, Grammajukku Formation	0.14–0.21 (0.17 ± 0.03, 2)	−31.5 to −29.5 (−30.5 ± 1.0, 2)	0.03	3.0–3.2 (3.1 ± 0.1, 2)
ASF6	Gray shale, Grammajukku Formation	0.18–0.20 (0.19 ± 0.01, 2)	−30.3 to −30.0 (−30.1 ± 0.1, 2)	0.04	2.9–3.1 (3.0 ± 0.1, 2)
ASF8	Gray shale, Grammajukku Formation	0.12 (1)	−30.1 (1)	0.07	2.4–2.6 (2.5 ± 0.1, 2)
ASF2	Green shale, Grammajukku Formation	0.17 (1)	−29.2 (1)	0.03	2.1–2.3 (2.2 ± 0.1, 2)
ASF3	Green shale, Grammajukku Formation	0.14 (1)	−30 (1)	0.04	3.3–3.4 (3.3 ± 0.1, 2)
		0.16 ± 0.02 ($n = 8$)	−30.4 ± 1.0 ($n = 8$)	0.05 ± 0.01 ($n = 12$)	2.8 ± 0.4 ($n = 12$)

prevalent biochemical process compared to normal marine production during shale deposition. This process was identified as dominating the N cycle in stratified early Cambrian oceans with oxic surface waters and anaerobic conditions in the bottom waters (Beaumont and Robert 1999; Cremonese et al. 2013; Spangenberg et al. 2014; Ader et al. 2014).

The Alum Shale Formation was deposited in a shallow sea overlying the lower Cambrian transgressive siliciclastic

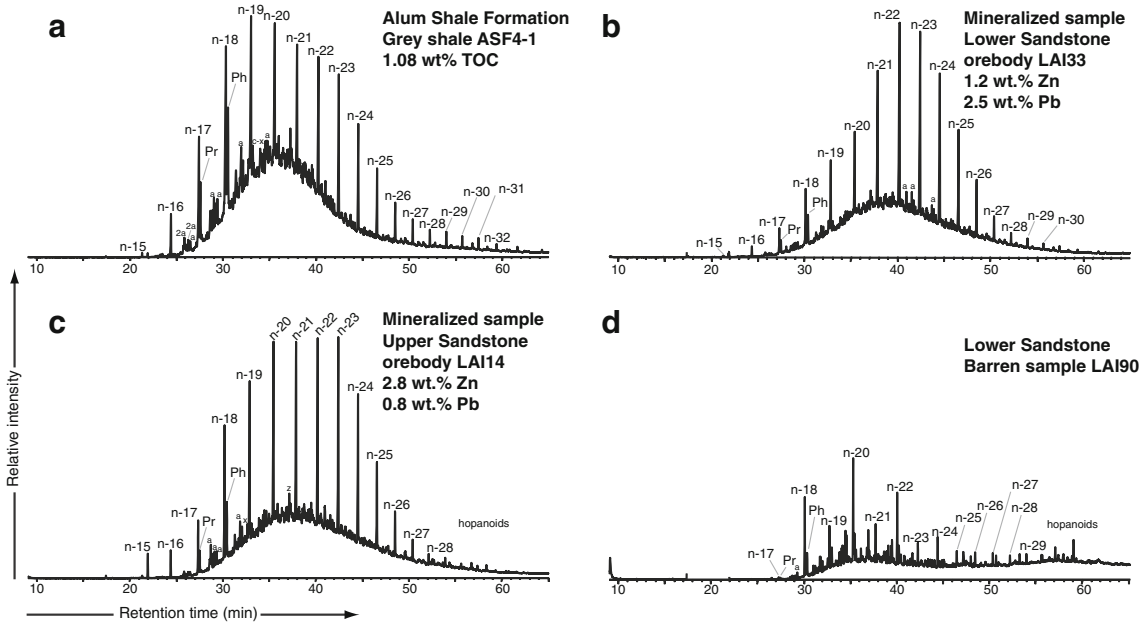

Fig. 10 Total ion chromatograms (TIC), obtained by gas chromatography-mass spectrometry (GC-MS) of the saturated hydrocarbon fraction of organic solvent-extractable bitumen, show dominance of normal alkanes (n-x, x = number of carbon atoms) in mineralized and barren samples at Laisvall. **a** Organic-rich shale in the Alum Shale Formation, **b** Lower Sandstone, **c** Upper Sandstone, and **d** Barren Lower Sandstone. The branched alkanes pristane (2,6,10,14-tetramethylpentadecane) and phytane (2,6,10,14-tetramethylhexadecane) from the compound class of regular isoprenoid hydrocarbons are also present. Cyclic alkanes forming rings of six carbon atoms (cyclohexane) were detected in some samples. Molecular ratios such as pristane/phytane and carbon preference index (CPI) were calculated from the area below the peaks. Abbreviations: C_x *n*-alkanes with x as C number, *Pr* pristane, *Ph* phytane

Table 4 Distribution of hydrocarbons and selected biomarker parameters in organic-rich shale samples of the Alum Shale Formation, mineralized samples of the Upper Sandstone and Lower Sandstone orebodies at Laisvall, and a barren Lower Sandstone sample from an outcrop located 5 km north of the Laisvall mine

Samples and lithology	*n*-alkanes (maxima)	CPI	Pr/Ph	Pr/*n*-C_{17}	Ph/*n*-C_{18}
Organic-rich shale (1.08 wt% TOC), Alum Shale Formation (ASF4-1)	C_{16}–C_{32} (C_{19}–C_{20})	1.04	0.39	0.62	0.65
Organic-rich shale (1.08 wt% TOC), Alum Shale Formation (ASF4-2)	C_{16}–C_{32} (C_{19}–C_{20})	0.95	0.51	0.62	0.60
Sphalerite-galena mineralized Upper Sandstone orebody (LAI14)	C_{16}–C_{28} (C_{20}, C_{21}, C_{22}, C_{23})	0.95	0.38	0.70	0.55
Galena ± sphalerite mineralized Lower Sandstone orebody (LAI33)	C_{17}–C_{30} (C_{22}–C_{23})	0.93	0.44	0.71	0.62
Barren Lower Sandstone (LAI90)	C_{18}–C_{29} (C_{20})	0.55	0.05	1.00	0.52

CPI carbon preference index for *n*-alkanes calculated as the sum of odd carbon number to the sum of even carbon number over the total carbon number range, *Pr* pristane, *Ph* phytane

sequence comprising subtidal shale, phosphorite lag, and a fluvial-beach-tidal sandstone complex (Willdén 1980; Thickpenny 1984). The stratigraphic sequence bears similarities with the Precambrian Baraga Group, Michigan, USA

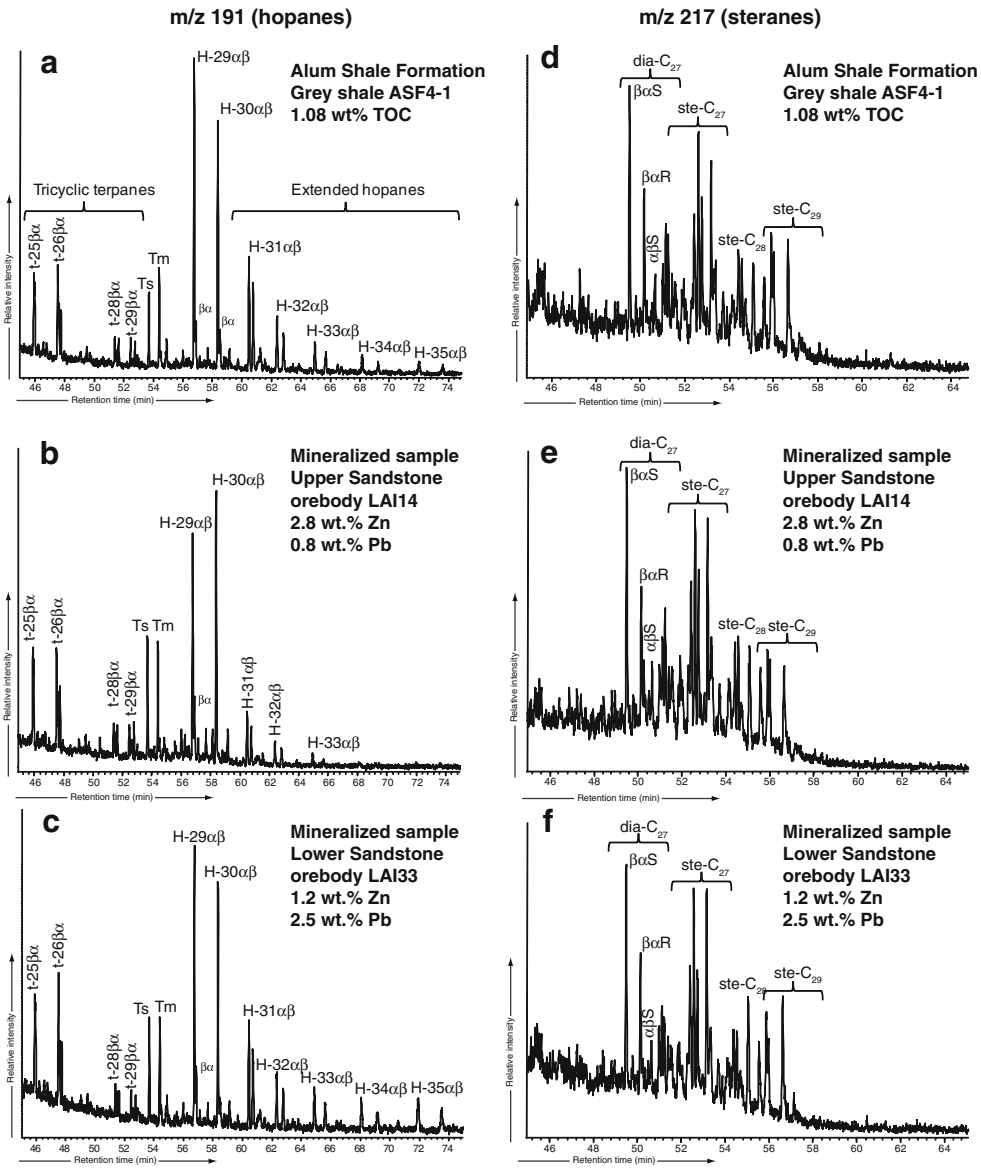

Fig. 11 Representative distribution of hopanes (diagnostic ion having a mass to charge ratio *m/z* of 191) and steranes (diagnostic ion having a *m/z* ratio of 217) in the saturated hydrocarbon fraction of organic solvent-extractable bitumen obtained by gas chromatography-mass spectrometry (GC-MS) in the following samples at Laisvall: **a**, **d** organic-rich shale in the Alum Shale Formation; **b**, **e** Upper Sandstone; **c**, **f** Lower Sandstone. Abbreviations: *x* number of carbon atoms; *t-xβα* 13β(H), 14α(H) tricyclic terpanes; *Ts* 18α(H)-22,29,30-trisnormeohopane; *Tm* 17α(H)-22,29,30-trisnorhopane; *H-xαβ* 17α(H), 21β(H)-hopanes; *H-xβα* 17β(H), 21α(H)-hopanes; *dia-xβα* 13β(H), 17α(H) diasteranes, S and R epimer configuration at C-27; *dia-xαβ* 13α(H), 17β(H) diasteranes; *ste-C_x* steranes

(Nelson et al. 2010; Peir Pufahl, 2014, personal communication), and suggests continuous continental input of nutrients (N, P, trace elements) associated with increased weathering. Our new biogeochemical data suggest that the middle Cambrian to Lower Ordovician epicontinental sea, in which the Alum Shale Formation was deposited, may have been characterized by oxic surface waters and anaerobic conditions in the bottom waters. Deposition of pyrite- and organic-rich ^{13}C-depleted carbonaceous shales of the Alum Shale Formation would illustrate rapid organic C burial with development of an anoxic/euxinic sediment-water interface (e.g., Spangenberg et al. 2014). The higher $\delta^{34}S$ values in pyrite (14.5 to 16 ‰) in the Alum Shale Formation immediately above sandstone at Laisvall compared to pyrite $\delta^{34}S$ values at Vassbo (6.8 to 7.6 ‰) might reflect the expansion of euxinic conditions during deposition of this formation. Indeed, Gill et al. (2010) showed that a peak of sulfur isotope excursions for pyrite in the Cambrian Alum Shale Formation coincided with a large and rapid excursion in the marine carbon isotope record thought to be indicative of a global carbon cycle perturbation. Strongly redox-stratified and eutrophic basins of lower Cambrian age were also described in the area of Lake Mjøsa in southern Norway (e.g., Vidal and Nystuen 1990).

Sandstone burial and P-REE-Ti mineral association

The present work has identified significant amounts of anatase, monazite, fluorapatite and, to a lesser extent, xenotime in the ore-bearing sandstone units, in particular the Upper Sandstone at Laisvall. The depositional environment of the Alum Shale Formation may explain the formation of these authigenic P-REE-Ti minerals in several parts of the Upper Sandstone beneath the sediment-water interface during sandstone burial. Aluminophosphates and xenotime in similar concentrations (<0.05 vol%) but smaller sizes (<0.1 to 10 μm) than at Laisvall (50 to 450 μm) were reported in marine sandstone of Archean to Cretaceous ages in Australia where they were shown to result from early diagenetic processes (Rasmussen, 1996). In accordance with the work of Rasmussen (1996) and Nelson et al. (2010), the following sequence of events can be proposed for the Upper Sandstone at Laisvall (Fig. 12).

In the oxic zone of sandstone (Fig. 12a), decomposition of organic matter released phosphorous that was adsorbed along with REEs onto newly formed Fe-(oxyhydr)oxides. Concurrently, anatase precipitated and enclosed detrital quartz, zircon and monazite. In the anoxic zone of sandstone (Fig. 12b, c), Fe-(oxyhydr)oxides were no longer stable. Iron was therefore fixed in pyrite that formed from hydrogen sulfide produced during decomposition of organic matter (e.g., pyrite with $\delta^{34}S$ value of −6.4 ‰ in the Upper Sandstone). REEs and P released from Fe-(oxyhydr)oxides and clay particles precipitated as authigenic monazite associated with

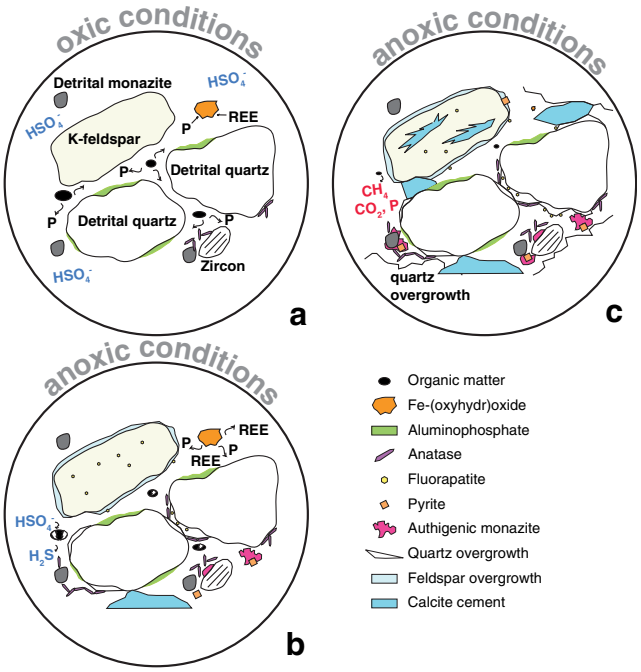

Fig. 12 Schematic diagrams showing the dominant mineralogical precipitation reactions during sandstone burial in oxic conditions (**a**) or anoxic conditions (**b**, **c**) in the Upper Sandstone during deposition of the middle Cambrian to Lower Ordovician Alum Shale Formation. **a** P and REE are adsorbed onto Fe-oxyhydroxides. Anatase is precipitated as needles coating quartz, while P is released during reactions of organic matter maturation. **b** With establishment of anoxic conditions, Fe-oxyhydroxides start being unstable. Fluorapatite and authigenic monazite (*pink*) are precipitated locally associated with pyrite formed from bacterial sulfate reduction. **c** With established anoxic conditions, P and REE are totally desorbed from Fe-oxyhydroxides that are no longer stable. Fe is fixed in pyrite, whereas P and REE are fixed in authigenic monazite. Calcite forms a major cement of sandstone

pyrite (Fig. 6b) and fluorapatite precipitated from fluorine in connate seawater. With continuous burial, xenotime outgrowths may have formed on detrital zircon (e.g., Fig. 6a). A similar mineral association was described at the Magellan MVT Pb deposit in the Paleoproterozoic Earaheedy Basin in Western Australia (Muhling et al. 2012), where authigenic monazite grains were successfully dated by SHRIMP and gave a lower age limit for MVT mineralization. However, monazite grains in the Upper Sandstone orebody at Laisvall could not be dated because the grains were too small to be separated and most grains contained micrometer-size galena that would have complicated interpretation of U-Pb analyses (Fig. 6b).

In the Lower Sandstone at Laisvall, Ba-bearing K-feldspar overgrowths around K-feldspar detrital grains and the absence of barite attest to the presence of Ba-bearing and sulfate-poor hydrothermal fluids. In this unit and in the sandstone at Vassbo, precipitation of fluorapatite on the rims of K-feldspar grains and as a coating on detrital quartz grains, as well as the preservation of fossil phosphate fragments (Figs. 8g, h and 6d) suggest relatively alkaline pH conditions

(Ben Hassen et al. 2010). The coeval precipitation of framboidal pyrite is consistent with anoxic conditions.

Calcite and barite cementation and porosity generation for subsequent Pb-Zn mineralization

The local occurrence of manganiferous calcite is typical of precompaction calcite cement in sandstone reservoir, such as in the Albert Formation reservoir sandstone, New Brunswick, Canada (Chowdhury and Noble 1996). Extensive calcite cementation was accompanied by pyrite precipitation in all studied sandstone aquifers (Fig. 3).

Serrated and etched edges of calcite cement are evidence of its local dissolution at the onset of or during barite precipitation at slightly more acidic pH. Partial dissolution of K-feldspar in the Lower Sandstone at Laisvall and the sandstone at Vassbo produced additional porosity during calcite and barite precipitation (Fig. 4a).

Precipitation of calcite and barite cements, in contrast to quartz cementation, may leave some intercrystalline porosity in sandstone paleoaquifers and enable fluid movement by capillarity (Surdam and Yin 1993). In addition, subsequent partial dissolution of calcite and barite provides a potential for permeability necessary for mineralization at a later stage (Figs. 4 and 5c). Surdam and Yin (1993) described the importance of carbonate cement that ensures the preservation of intergranular volume of porosity and, in part, original porosity (Fig. 4). At Laisvall and Vassbo, available porosity for epigenetic mineralization was about 29 vol% in sandstone paleoaquifers with widespread calcite and barite cements, locally replaced subsequently by Pb-Zn sulfides (Fig. 4a). By contrast, porosity at the onset of the pre-Pb-Zn sulfide stage was as low as 8 vol% in sandstone dominated by quartz cement and lacking calcite and barite cements (Fig. 4b).

The $\delta^{18}O_{PDB}$ values (−22 to −14 ‰, Fig. 13, cf. original SMOW data in Rickard et al. 1979; Wallin 1982; Broman 1983) of calcite cements at Laisvall and Vassbo are ^{18}O-depleted compared with the O isotope values of −10 to −7 ‰ reported for Cambrian to Ordovician seawater and carbonate rocks (cf. Veizer et al. 1999; Veizer 2004; Ishikawa et al. 2008; Prokoph et al. 2008). Menotti (2006) interpreted "anomalous" and relatively depleted $\delta^{18}O$ values (−14 to −10 ‰) of carbonate rocks of the Taconic passive margin of Laurentia (upper Cambrian), New York, USA, as illustrating an overprint on the primary oxygen signal by ^{18}O-depleted water during diagenesis. Porous and permeable calcite-cemented sandstones at Laisvall and Vassbo were prone to exchange with diagenetic fluids and crystallization of ^{18}O-depleted calcite.

Hydrocarbon origin and migration

The pronounced differences in gas chromatograms of the mineralized and barren sandstone samples indicate that hydrocarbons involved in the mineralizing processes were not derived from scarce kerogen indigenous to the sandstone (Figs. 10 and 11). The similarity of the hydrocarbon distributions (Figs. 10 and 11) of the organic-rich shale of the Alum Shale Formation and the mineralized sandstone samples, the common algal and bacterial source of organic matter for the derivatives found in these samples, and the lack of other potential hydrocarbon source rock in the stratigraphy in the region suggest that the Alum Shale Formation was the source of hydrocarbons and other organic compounds (organic acid anions) that migrated

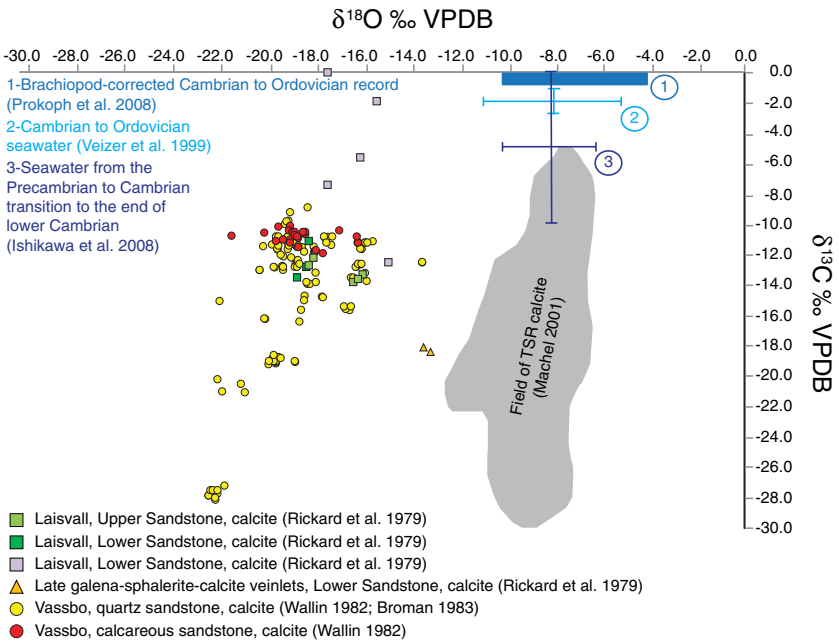

Fig. 13 $\delta^{13}C$ VPDB vs. $\delta^{18}O$ VPDB plot of calcite from the orebodies at Laisvall and Vassbo. Data compiled from the literature for Laisvall (Rickard et al. 1979) and Vassbo (Wallin 1982; Broman 1983). The empirical fields of TSR-produced calcite (Machel 2001), brachiopod-corrected Cambrian to Ordovician record (Prokoph et al. 2008), Cambrian to Ordovician seawater (Veizer et al. 1999), and seawater from the Precambrian-Cambrian transition to the end of the lower Cambrian (Ishikawa et al. 2008) are shown for reference

into sandstone and were involved in the mineralizing processes for Pb-Zn mineralization at Laisvall.

Hydrocarbon generation necessitates that carbonaceous shales from the Alum Shale Formation were buried and heated sufficiently (>60 °C) to enter the oil window. We propose that hydrocarbons were generated by carbonaceous shales in the Alum Shale Formation during burial within the early Caledonian foreland basin, situated to the northwest of the continental passive margin of Baltica and the locations of the Laisvall and Vassbo deposits (Fig. 14; Saintilan et al. 2015b). It is suggested that hydrocarbon, which had entered sandstone in the foredeep, could migrate toward the craton and eventually accumulate to favorable locations/traps to the southeast (Laisvall and Vassbo, Fig. 14a–c). At 467 ± 5 Ma (Middle Ordovician), the proposed age for sphalerite mineralization at Laisvall (Saintilan et al. 2015b), favorable settings may have allowed the accumulation of hydrocarbons in trap sites located ~20 km southeast of the forebulge and the edge

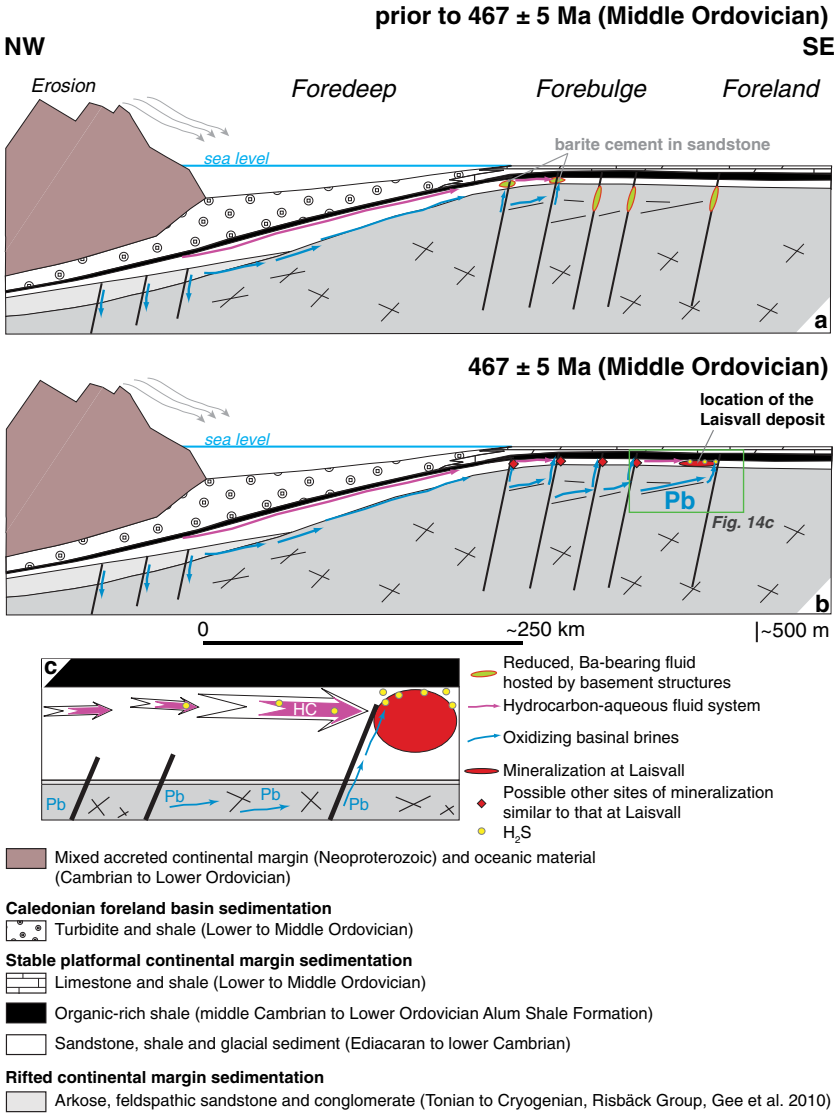

Fig. 14 Genetic model for the Laisvall deposit in a foreland basin setting during early Caledonian orogenic activity (upper Cambrian to Middle Ordovician). **a** Paleotectonic setting prior to mineralization at Laisvall (467 ± 5 Ma) in the Middle Ordovician. **b** Paleotectonic setting during mineralization in the Middle Ordovician. NW-SE paleocross-section showing the location of the present-day Laisvall deposit ~20 km SE of the edge of the basin and its forebulge (after Greiling and Garfunkel 2007; Saintilan et al. 2015b). Reactivation of basement structures that cut Ediacaran to Cambrian sandstone in the Phanerozoic (e.g., faults in the basement at Laisvall) occurred close to the forebulge (Saintilan et al. 2015a, b). Migration of hydrocarbons from organic-rich shales of the Alum Shale Formation occurred during burial and heating in the foredeep beneath syn-orogenic and pre-orogenic sediments and the accretionary load (Saintilan et al. 2015b; this study). Hydrocarbons migrated into Ediacaran to Cambrian sandstones, and then into sandstones toward the craton, and finally accumulated in favorable traps (e.g., at the Laisvall deposit). It is possible that similar trap sites favorable for mineralization existed to the west of the site of mineralization at Laisvall. Mineralization corresponding to these trap sites might be present in either autochthonous sandstone or in sandstone in the lowermost allochthonous units inside the Caledonian orogen. **c** Close-up of the mineralizing process at Laisvall

of the early Caledonian foreland basin, which corresponds to the present-day location of the Laisvall deposit (Fig. 14b, c).

Pb-Zn mineralization

Presulfide stage barite precipitation

The range of $\delta^{34}S$ values of barite in the Lower Sandstone and Upper Sandstone orebodies at Laisvall (14 to 32.7 ‰, Fig. 9) suggests that sulfate in barite was derived from (i) Cambrian to Ordovician seawater (range 27 to 33 ‰; Claypool et al. 1980) present or migrating in permeable sandstone paleoaquifers, which was locally diluted by (ii) formation waters with sulfate derived from the oxidation of pyrite in organic-rich shale in the overlying Alum Shale Formation (range 14.5 to 16.0 ‰; Rickard et al. 1979). This interpretation is supported by the fact that sulfur isotope fractionation during precipitation of sulfate minerals from dissolved sulfate is small (<0.5 ‰; Ohmoto and Rye 1979).

The new $^{87}Sr/^{86}Sr$ ratios of barite in the Upper Sandstone and Lower Sandstone orebodies (0.718791 ± 14 and 0.722349 ± 14, respectively) are much higher than the $^{87}Sr/^{86}Sr$ ratios of Cambrian to Ordovician seawater (around 0.709; Veizer et al. 1999). These $^{87}Sr/^{86}Sr$ ratios, the $^{40}Ar/^{36}Ar$ ratios (range 4000–6500), and the high concentrations of $^{40}Ar^*$ in fluid inclusions preserved in barite at Laisvall (Kendrick et al. 2005) suggest that these fluids had a long premineralization crustal residence time (in the order of 100 Ma; Kendrick et al. 2005; this study). In addition, fluid inclusions in barite have salinities of 18 ± 8 wt% NaCl eq. and Br/Cl ratios of c. 3 to 5×10^{-3} (Kendrick et al. 2005).

The current model proposes that crustal, saline, Ba-bearing and sulfate-poor fluids in equilibrium with Paleoproterozoic basement rocks resided in structures in the basement. Upon cratonward migration of oxidizing basinal brines derived from the early Caledonian foreland basin during the Middle Ordovician, the Ba-bearing fluids at Laisvall were forced and expelled upward from their host structures into the overlying sandstone along reactivated steeply dipping faults in the basement (Saintilan et al. 2015a; Fig. 14a).

Barite precipitated in sandstone upon mixing of the reduced, neutral, Ba-bearing fluids with the above-described sulfate pool present in Ediacaran to Cambrian sandstone. The unusually high I/Cl values ($60–1600 \times 10^{-6}$) in fluid inclusions in barite at Laisvall (Kendrick et al. 2005) suggest that fluids involved in the pool of sulfate in Ediacaran to Cambrian sandstones must have interacted with I-rich organic matter in organic-rich sedimentary rock in the subsurface. It is possible that formation waters, which diluted connate Cambrian to Ordovician seawater in Ediacaran to Cambrian sandstone, interacted with I-rich organic matter and oxidized pyrite from the carbonaceous shale of the Alum Shale Formation during migration in the subsurface.

The similarity of $\delta^{34}S$ values of barite and the noble gas and halogen compositions of fluid inclusions in barite at Osen, Vassbo, and Laisvall (Fig. 9 and Kendrick et al. 2005) suggests a homogeneous fluid-flow model for basement-hosted Ba-bearing fluids at a regional scale. Pre-Pb-Zn sulfide stage barite cementation is a key feature common to several sandstone-hosted Pb-Zn deposits along the erosional front of the Caledonian orogen (Osen, Vassbo, Laisvall).

Sources of metal-bearing brines and their resurgence in sandstone

The results of microthermometry, noble gas, and halogen analyses in fluid inclusions in sphalerite and galena at Laisvall and Vassbo (Lindblom 1986; Kendrick et al. 2005) suggest that saline (c. 24 wt% NaCl eq., Br/Cl of c. 8×10^{-3} much greater than seawater), crustal fluids involved in mineralizing processes interacted with basement rocks ($^{40}Ar/^{36}Ar$ ratios of c. 500 to 1800; low to moderate $^{40}Ar^*$ concentrations; Kendrick et al. 2005). The initial $^{87}Sr/^{86}Sr$ ratio for sphalerite (0.7159000 ± 60, Saintilan et al. 2015b) may be close to the $^{87}Sr/^{86}Sr$ ratio for these evolved basement-interacted fluids.

These geochemical data, combined with the geodynamic setting proposed for the timing of mineralization at Laisvall as a response to early Caledonian orogenic activity (Saintilan et al. 2015b), suggest that the fluids originated as basinal brines. These brines resided in and interacted with pre-Ediacaran, rift-related feldspathic sandstones and arkoses. These rocks, containing detritus from the Baltica continent (Risbäck Group, Gee et al. 2010), were preserved in the deeper part of the early Caledonian foreland basin (Fig. 14a, b; Saintilan et al. 2015b).

Basinal brines flowed cratonward along the lower units of the basin, along the unconformity between Ediacaran to Cambrian sediments and the crystalline basement, and along fractures and gently dipping sheet joints in the upper part of the basement (Fig. 14b, c). The evolved basinal brines at the site of deposition had temperatures around 120 to 180 °C as determined by fluid inclusions in sphalerite (Lindblom 1986) and, consequently, probably had higher temperatures when they migrated through the Baltica basement. These oxidizing and saline fluids had the potential for transporting metals (Lindblom 1986; Kendrick et al. 2005). Lead radiogenic isotope data indicate that metals were derived primarily from basement rocks and their erosional products (Rickard et al. 1981; Johansson and Rickard 1984; Romer 1992; Saintilan 2015). At Laisvall, these evolved metal-bearing brines resurged toward the Middle Ordovician along reactivated steeply dipping faults in the basement that also affected the Ediacaran to Cambrian sandstones (Fig. 14b, c; Saintilan et al. 2015a, b).

Upon termination of the flow of oxidizing basinal brines cratonward, hydrodynamics was progressively restored to

equilibrium and the plumbing system returned to a situation of fluids in equilibrium with basement rocks. This hypothesis is supported by field evidence of calcite-fluorite ± pyrite veins hosted by fractures in the basement of the Laisvall deposit in the proximity of the main feeder faults (Saintilan et al. 2015a). Saintilan (2015) suggested that these basement veins formed during large-scale fluid flow from reduced and basement-interacted hydrothermal fluids that were in equilibrium with basement rocks.

Sources of hydrogen sulfide

The relatively small range of heavy $\delta^{34}S$ values (average 24–29 ‰) for most Pb-Zn sulfides samples (Fig. 15) suggests that most H_2S in the mineralizing fluid was produced during thermochemical sulfate reduction (TSR, Krouse et al. 1988; Machel 2001; Anderson 2008) of mainly Cambrian to Ordovician seawater sulfate with oxidation of organic compounds (hydrocarbons). Fractionation between TSR-produced H_2S in the fluid and H_2S fixed in sphalerite is negligible. Thus, the isotopic composition of sulfur in sphalerite should indicate the isotopic composition of sulfur in the fluid (cf. Ohmoto and Rye 1979). A schematic net mass balance of the TSR reaction was proposed by Machel (1987, 2001): hydrocarbons + HSO_4^{2-} → altered hydrocarbons + solid bitumen + $H_2S(HS^-)$ + $HCO_3^-(CO_2)$ (+H_2O).

The heaviest sulfur isotope composition corresponds petrographically to sphalerite (range 29 to 33 ‰) and galena (range 22 to 29 ‰) in the pores between quartz grains and is interpreted as the product of thermochemical reduction of aqueous sulfate with a composition of Cambrian to Ordovician seawater (27 to 33 ‰; Claypool et al. 1980). The rest of the spectrum of sulfur sphalerite isotope values corresponds to sphalerite formed by thermochemical reductive dissolution of barite (described in detail below) which has sulfate values between 14 and 33 ‰ (Table 1). Hydrogen sulfide produced by TSR was subordinately consumed by minor pyrite, showing $\delta^{34}S$ values between 30.5 and 32.5 ‰ (Fig. 9, Table 1), prior to extensive consumption of TSR-produced hydrogen sulfide by galena and sphalerite.

Textural and geochemical evidence (Figs. 8 and 9) indicates that a subordinate source of hydrogen sulfide for Pb-Zn sulfide precipitation with sulfur isotope compositions of 21 to 27 ‰ at Laisvall and 12 to 18 ‰ at Vassbo was the replacement, at an early stage, of euhedral to subhedral pyrite ± framboidal pyrite (Fig. 15). A third subordinate and localized source of hydrogen sulfide was identified at Laisvall in the feeder fault zone area (e.g., Fig. 16) of the Central Malm (Saintilan et al. 2015a) where sphalerite has $\delta^{34}S$ values around 2 ‰ (Fig. 15) that may be explained by reduced sulfur derived from sulfides (pyrrhotite, pyrite) in crystalline basement rocks.

An estimate of the fractions of H_2S derived from TSR on the one hand and pyrite replacement on the other hand is based on the distribution of sulfur isotope values and constraints from petrographic observations and QEMSCAN image analysis. It is suggested that TSR was the main source of hydrogen sulfide at Laisvall (~90 vol%) and Vassbo (~70 vol %), whereas pyrite replacement amounted to ~10 vol% at Laisvall and ~30 vol% at Vassbo.

The oxidation of organic compounds during TSR produces ^{13}C-depleted dissolved inorganic carbon, which may precipitate calcite with low $\delta^{13}C$ values (TSR-calcite; cf. Machel 1987, 2001). Previous stable C and O isotope studies at Vassbo (Wallin 1982; Broman 1983) reported data for calcite in the sandstone orebody and the underlying essentially barren calcareous sandstone (Fig. 2b). Although these analyses were not constrained petrographically, the following three calcite groups could be distinguished on the basis of their C isotope composition (Fig. 13): (1) −15 to −8 ‰, (2) −22 to −18 ‰, and (3) −30 to −28 ‰. Group 1 is common to both the sandstone orebody and the barren calcareous sandstone and thus

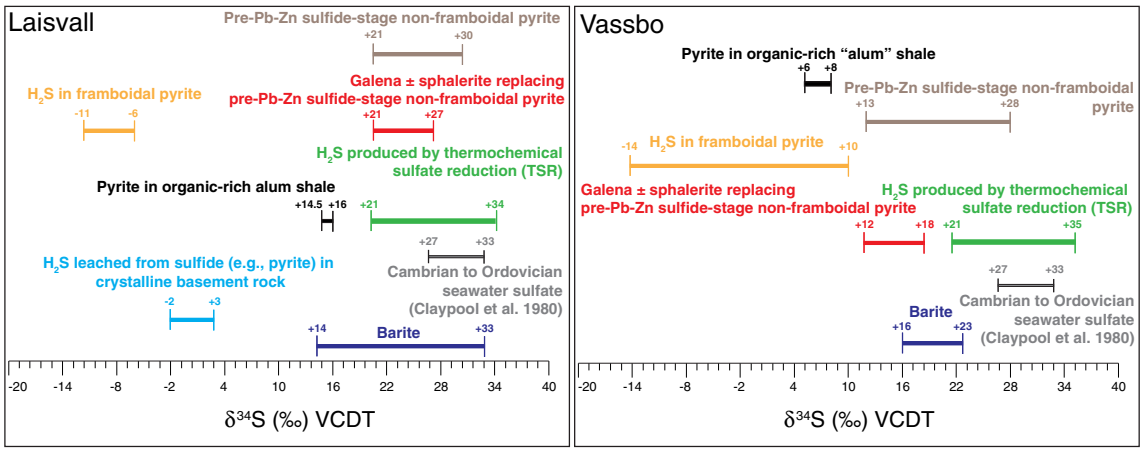

Fig. 15 Ranges of sulfur isotope composition in sulfides and barite at Laisvall and Vassbo compared with the compositions of possible sources of reduced sulfur

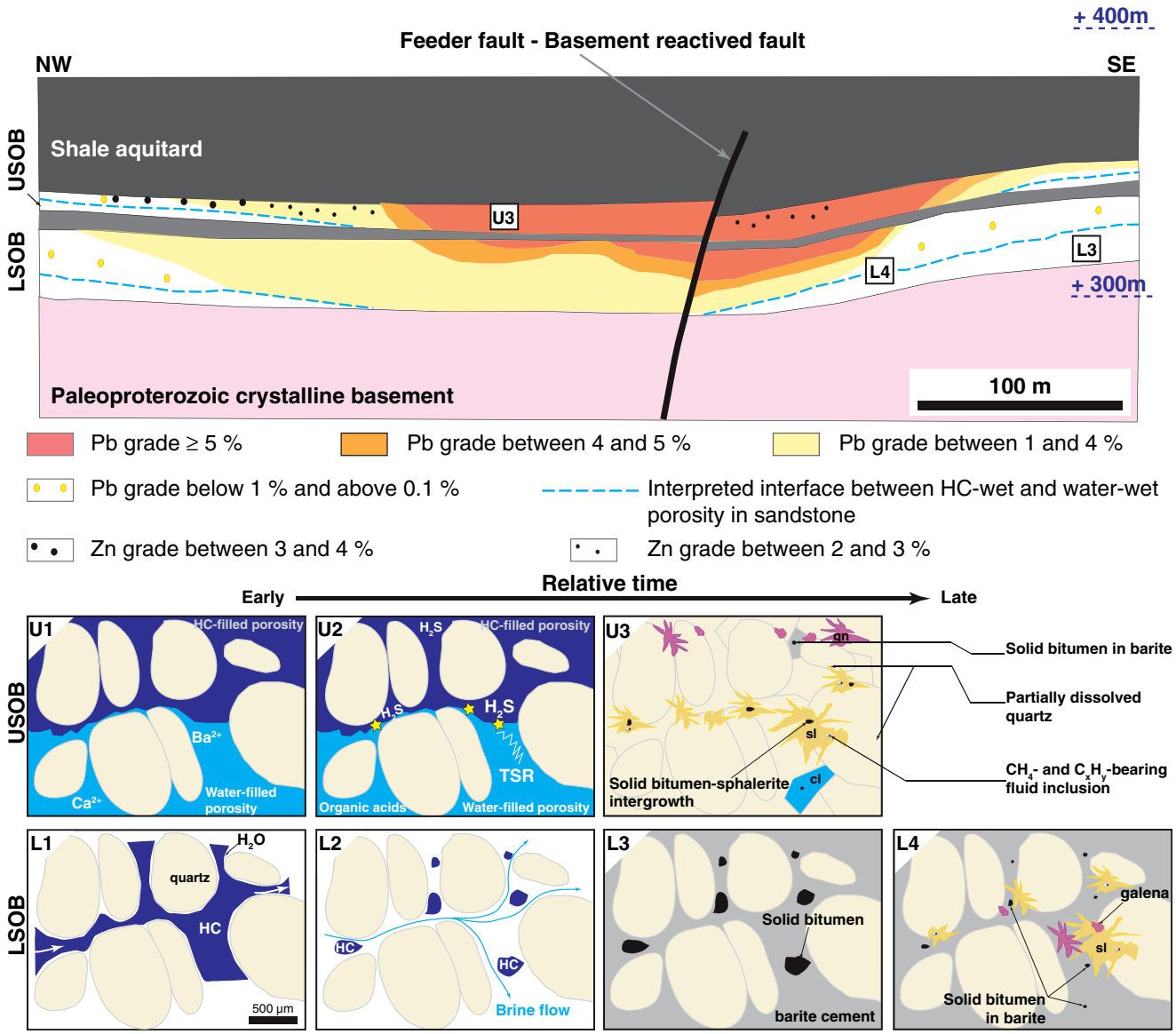

Fig. 16 NW-SE cross-section across the Nadok feeder fault system (between c. 300 and 400 m above sea level) showing the Pb-Zn grade distribution in the Upper Sandstone and Lower Sandstone orebodies (USOB and LSOB) separated by the relatively impermeable Middle Sandstone (modified after Saintilan et al. 2015a). Situations L1, L2, U1, and U2 illustrate processes leading up to and during mineralization. Situations L3, L4, and U3 correspond to mineralized and barren parts as observed today in macroscopic and microscopic samples. The locations L3, L4, and U3 are shown on the section. Diagrams show styles of porosity filling in the water-hydrocarbon system in the paleoaquifers at Laisvall and Vassbo, as deduced from textural evidence, occurrence of solid organic matter, and sulfur isotope composition of barite and Pb-Zn sulfides. Hydrocarbon (*HC*) can be oil or gas. L1: Parts of sandstone paleoaquifers were HC-wet following exogenous hydrocarbon migration. L2: Flow of aqueous fluids altered hydrocarbons, isolated hydrocarbon droplets and resulted in the formation of solid bitumen. L3: Prior to or as thermochemical sulfate reduction proceeded and produced H_2S, barite cement precipitated, and enclosed solid bitumen. L4: Pb-Zn sulfides precipitated from H_2S produced during reductive dissolution of barite by organic acids. Some quartz dissolution coeval with barite dissolution accommodated secondary porosity for Pb-Zn sulfide precipitation (see also Fig. 17 and text for explanation). U1: Parts of the paleoaquifers showed porosity stratification with an HC-wet part underlain by a water-wet part. U2: TSR occurred at the interface between the HC-filled porosity and the water-filled porosity and H_2S was produced (after Machel 2001; Anderson 2008). U3: Upward migration, fluctuation of the hydrocarbon-water interface, and formation of H_2S along this interface may explain the alternating layers of galena and sphalerite

might correspond to pre-Pb-Zn sulfide stage calcite cement common to these horizons. A preferred hypothesis is that the C isotopic composition of group 1 calcite reflects dissolved inorganic carbon resulting from the oxidation of organic compounds reflecting processes before Pb-Zn mineralization, possibly diagenetic processes. On the other hand, the occurrence of strongly ^{13}C-depleted calcite (groups 2 and 3) in the sandstone orebody at Vassbo may correspond to subhedral TSR-calcite that was identified in the current study. By contrast, the orebodies at Laisvall are characterized by a paucity

of ore-stage calcite, which is fine-grained and intimately intergrown with Pb-Zn sulfides (Fig. 7f, g). C isotope data are lacking for this calcite.

Formation of solid bitumen, timing of TSR, and TSR reaction zones

Two types of solid bitumen are present in the orebodies at Laisvall: (i) solid bitumen intergrown with sphalerite in the Upper Sandstone orebody and (ii) solid bitumen inclusions in barite cement and, in a few places, in fluorite or calcite cements in the Lower Sandstone orebody. The timing of TSR (mainly before and to some extent during Pb-Zn mineralization) and the size and location of TSR reaction zones can be estimated from these petrographic observations.

Timing of TSR

Efficient TSR requires temperatures of at least 100 to 140 °C (Machel 1987; Heydari and Moore 1989; Goldhaber and Orr 1995; Worden et al. 1995; Simpson et al. 1996; Machel 2001, Anderson 2008) and pH values of 4 to 8. Temperatures of 120 to 180 °C during mineralization have been proposed on the basis of fluid inclusion studies in sphalerite at Laisvall (Lindblom 1986), whereas lines of evidence for slightly acidic conditions during mineralization are given by the presence of sericite in sphalerite and galena (Fig. 7d, e) and the paucity of ore-stage calcite.

Intimate intergrowth of solid bitumen with sphalerite in the Upper Sandstone orebody (Fig. 8a) suggests that this bitumen formed during the main stage of Pb-Zn mineralization. Given that the main source of hydrogen sulfide at Laisvall was TSR, this bitumen is interpreted as a by-product of TSR. This suggests that TSR may have occurred before and during Pb-Zn mineralization. This scenario is compatible with the experimental results by Thom and Anderson (2008) that indicate that TSR may occur during mineralization in MVT deposits.

It is critical to understand the timing of hydrocarbon migration into the sandstones at the mineralization site and the time span needed for TSR to produce H_2S for the precipitation of Pb-Zn sulfides. Information is provided by the presence of solid bitumen inclusions in pre-Pb-Zn sulfide stage barite cement and more rarely in earlier calcite cement. It is possible that hydrocarbon migrated into the sandstone paleoaquifers prior to and during barite precipitation (Fig. 3; Fig. 16 situation L1). At Laisvall, it is proposed that the change of the main cement from calcite to barite is coeval with hydrocarbon migration in sandstone. With continuous flow of aqueous fluids in the bottom parts of paleoaquifers (e.g., the bottom part of the Lower Sandstone paleoaquifer at Laisvall, Fig. 16 situation L2), hydrocarbons were altered and solid bitumen formed and was included in barite ± fluorite (Fig. 16 situation L3). Simultaneously, in the higher parts of the sandstone paleoaquifers below the overlying aquiclude, TSR reaction zones between hydrocarbons and aqueous sulfate were preserved and H_2S could form and accumulate (Fig. 16 situations U1 and U2), whereas barite precipitated in the lower parts. This interpretation is supported by the morphology of the orebodies at Laisvall and Vassbo, where the highest grade ore zones occur in the roof of the sandstone paleoaquifers, reflecting the supply of H_2S for sulfide precipitation (Figs. 14c and 16; Saintilan et al. 2015a).

TSR reaction zones and layering of the ore

Machel (2001) stressed that TSR necessitates physical contact between hydrocarbon and aqueous sulfate based on the fact that the sulfate does not react by TSR in the solid state. Reduced sulfur could have been generated at Laisvall and Vassbo at the site of mineralization or west of it and subsequently transported to the mineralization site (Fig. 14c). TSR may have taken place before sulfide mineralization at the Laisvall ore site, where parts of the pores in the sandstone reservoirs (e.g., the Upper Sandstone orebody and several parts of the Lower Sandstone orebody) remained distinctly hydrocarbon-filled and underlain by parts with water-filled pores (Fig. 16 situations U1 to U3). In this situation, TSR would have been confined to a hydrocarbon-water interface. TSR may then occur throughout the entire hydrocarbon-containing part of the reservoir, if the irreducible water saturation (the fraction of the pore space occupied by water when hydrocarbon content is at maximum) is high (Machel 2001). Such ideal conditions may have prevailed in the Upper Sandstone and locally in the Lower Sandstone orebodies, where continuous, horizontal and alternating layers of galena and sphalerite are observed (Figs. 7a and 16 situation U3). Upward migration and fluctuation of the hydrocarbon-water interface and the formation of H_2S along this interface might explain the layering of the ore.

Reductive dissolution of barite and timing and origin of quartz dissolution

Barite cement and quartz in the Lower Sandstone orebody at Laisvall and the sandstone orebody at Vassbo were dissolved, and the porosity was filled in by sphalerite and galena. Given the necessity to have aqueous sulfate for TSR to take place (Machel 2001), this means that sulfate from barite dissolution was reduced in situ via TSR as it entered in solution (Fig. 16 situation L4).

Solubility of barite is favored by increasing salinity and decreasing temperature between 200 and 100 °C (Rimstidt 1977; Hanor 2000). In addition, organic acids can increase reservoir porosity by dissolving minerals (via

cation-organic acid anion complexation) or by increasing their dissolution rates (Knauss et al. 1997; Surdam et al. 1984; Greenwood et al. 2013). Chemical thermodynamic speciation modeling suggests that organic acids significantly influence the solubility of alkaline earths (Ba^{2+}; Knauss et al. 1997 in Greenwood et al. 2013). Organic acids are common by-products of the TSR reaction (Machel 2001). These organic acids are also present and highly soluble in low-salinity subsurface formation waters (Hanor 1996). Hence, it is probable that organic acids were present in sandstone before and during mineralization. Thus, we propose that dissolution of barite by organic acids resulted in barium and sulfate in solution at Laisvall and Vassbo. Sulfate could be reduced via TSR in the areas of barite dissolution and additional Pb-Zn sulfides precipitated. Similar reductive dissolution of barite was reported for stage 3 of sphalerite mineralization at the shale-hosted Zn-Pb-Ag Red Dog deposit, Alaska, USA (Kelley et al. 2004).

A temperature increase and complementary organic and inorganic processes can be advocated to explain the local quartz dissolution features mentioned above. Quartz dissolution, which locally created secondary porosity for mineralization (Fig. 17), is common and restricted to areas of reductive barite dissolution and/or in spaces where sulfides are intergrown with sericite (Figs. 3, 7b, c, and 16). Bennett (1991) showed that organic acid-rich aqueous systems can lower the activation energy of the chemical reaction of quartz dissolution by 20 % at neutral pH and temperature as low as 25 to 70 °C. Dissolution of quartz and its solubility might have been increased by organic acids that were either present in formation waters or were created as by-products of the TSR reaction.

Cations such as Ba^{2+} and K^{+} and to a lesser extent Ca^{2+} are known for their thermodynamic property (frequency of solvent exchange or K_{ex}) that lowers the activation energy for quartz dissolution (Dove and Nix 1997; Dove 1999). According to these authors, these cations favor quartz dissolution by enabling the protonation of Si-O bridging structures due to their tendency of high exchange rate at the quartz-solution interface. Barium cations could be placed in solution via reductive dissolution of barite at the time of Pb-Zn sulfide precipitation, while potassium and calcium cations were already in solution during the pre-Pb-Zn sulfide stage due to K-feldspar dissolution and calcite replacement by barite, respectively.

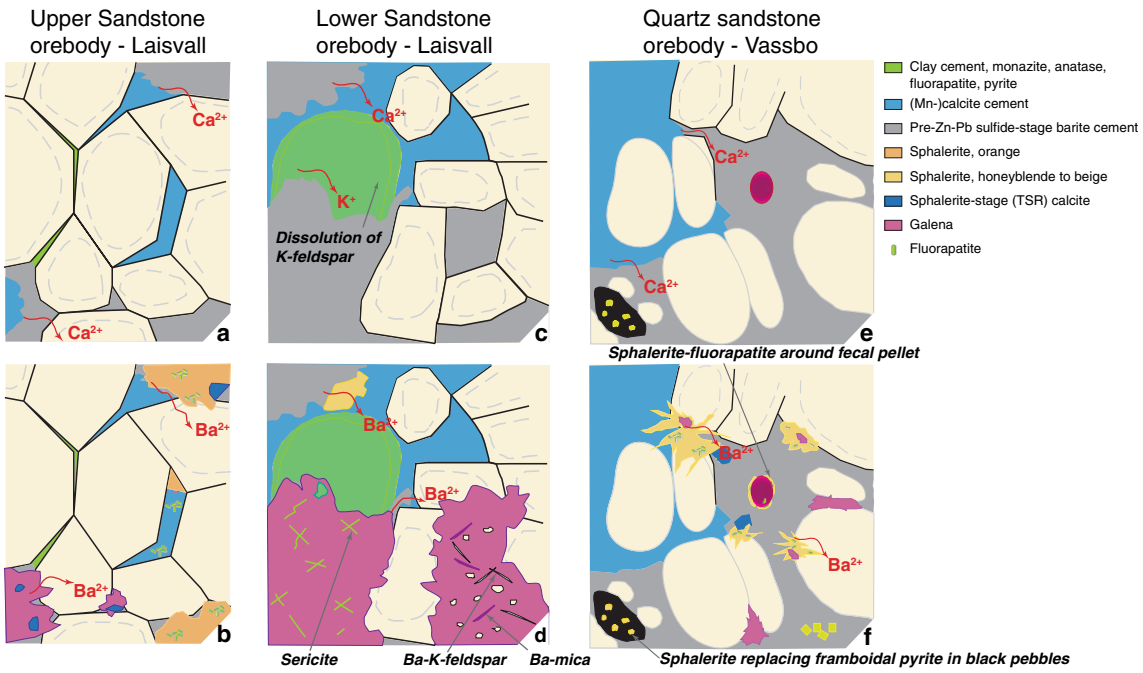

Fig. 17 Creation of secondary porosity for Pb-Zn sulfide precipitation by quartz (detrital quartz and overgrowth) dissolution due to local temperature increase; the thermodynamic property of Ba^{2+}, K^{+}, and Ca^{2+} cations known as "frequency of solvent exchange"; and the action of organic acids produced during thermochemical sulfate reduction (*TSR*). **a** Upper Sandstone orebody at Laisvall. Replacement of calcite by barite released Ca^{2+} cations into solution. **b** Reductive dissolution of barite produced H_2S_{TSR} that was consumed by sphalerite and galena precipitation, while Ba^{2+} and Ca^{2+} cations and organic acids contributed to quartz dissolution. **c** Lower Sandstone orebody at Laisvall. Dissolution of K-feldspar and replacement by barite. Calcite was also replaced by barite. K^{+} and Ca^{2+} cations were put into solution. **d** Reductive dissolution of barite produced H_2S_{TSR} for galena and sphalerite precipitation, while K^{+} and Ca^{2+} cations together with organic acids contributed to quartz dissolution. **e** Quartz sandstone at Vassbo. Same situation as in **a. f** Reductive dissolution of barite produced H_2S_{TSR} for sphalerite ± galena precipitation. Quartz dissolution was favored by the combined action of Ba^{2+} and Ca^{2+} cations and organic acids. Reductive dissolution of barite also occurred around fecal pellets cemented by barite

Conclusions

The current study has provided a genetic model for the Laisvall and Vassbo deposits in Sweden including building on and refining the two-fluid mixing models presented by Rickard et al. (1975, 1979), Lindblom (1986), and Kendrick et al. (2005). The model involves the mixing of metal-bearing basinal brines with a pool of H_2S in sandstone. Important new factors include the following:

- Barite and calcite cements that precipitated prior to the Pb-Zn sulfide stage represent a key feature of all Laisvall-type deposits (e.g., Laisvall, Vassbo, Osen). Calcite and barite protected sandstone from quartz cementation. The available porosity for epigenetic mineralization, including that produced by subsequent partial dissolution of calcite and barite cement, was almost four times higher in calcite- and barite-cemented sandstone paleoaquifers (29 %) compared to those mainly cemented by quartz (8 %).
- A peculiar P-REE-Ti authigenic mineral association comprising monazite, fluorapatite, and anatase in the Upper Sandstone at Laisvall reflects processes active during sandstone burial and anoxic conditions in sandstone influenced by the euxinic character of the overlying and regionally extensive Alum Shale Formation, which was deposited in a redox-stratified, epicontinental sea in the middle Cambrian to Lower Ordovician.
- The change from barite-calcite cementation to Pb-Zn sulfide precipitation in sandstone illustrates a major change in the plumbing system at Laisvall. It is proposed that the reactivated basement structures (Saintilan et al. 2015a) at Laisvall were initially used by Ba-bearing, reduced, and neutral fluids in equilibrium with basement rocks. Subsequently, slightly acidic metal-bearing brines migrated through the same plumbing system. The early Caledonian arc-continent collision can account for the necessary flow to prevent these brines from equilibrating with the basement rocks. Recognition of barite cements in sandstone outcrop or drillcore may be used as an exploration vector, since it could be spatially associated with fertile structures in the basement.
- As a response to the early Caledonian orogenic activity during the Middle Ordovician, hot (>120 to 180 °C), basement-interacted (initial Sr ratio in sphalerite of 0.7159, $^{40}Ar/^{36}Ar$ ratios of c. 500 to 1800; low to moderate $^{40}Ar^*$ concentrations), oxidizing, slightly acidic and saline brines (c. 24 wt% NaCl eq., Br/Cl of c. 8×10^{-3} much greater than seawater; Lindblom 1986; Kendrick et al. 2005; this study) flowed from the foreland basin toward the craton. These brines had the potential for transporting metals derived from basement rocks and their erosional products (Rickard et al. 1981; Johansson and Rickard 1984; Romer 1992; Saintilan 2015) and were mobilized along reactivated, steeply dipping faults that also affected sandstones in the forebulge to the foreland basin.
- The morphology of the orebodies at Laisvall and Vassbo (highest grade mineralization at the roof of the sandstone paleoaquifers) reflects the supply of H_2S in traps of accumulated hydrocarbon. Based on sulfur isotope compositions, the main source of hydrogen sulfide at Laisvall (average $\delta^{34}S = 24$ to 29 ‰) was produced in the sandstone during TSR with oxidation of exogenous hydrocarbons. Exogenous hydrocarbons migrated from source rocks in the middle Cambrian to Lower Ordovician Alum Shale Formation into sandstone where they accumulated in favorable traps underneath shale aquicludes. Hydrocarbons were generated in the organic-rich Alum Shales during burial and heating through the oil window in the foredeep of the early Caledonian foreland basin. The presence of solid bitumen inclusions in barite indicates that hydrocarbon migration had already started prior to or during barite-calcite cementation of the sandstone units. The occurrence of solid bitumen intimately intergrown with sphalerite suggests that a subordinate amount of H_2S was produced by TSR during Pb-Zn mineralization, as proposed by Thom and Anderson (2008) based on experimental result on the kinetics of TSR. The bulk of H_2S is inferred to have been produced by TSR prior to Pb-Zn mineralization.
- Continuous and horizontal layers of sulfides roughly parallel to bedding suggest that TSR took place at the hydrocarbon-water interface between distinctly hydrocarbon-filled and underlying water-filled parts of the porosity of the sandstone reservoirs. Upward migration, fluctuation of the hydrocarbon-water interface, and formation of H_2S along this interface may explain the alternating layers of galena and sphalerite.
- The source of aqueous sulfate which was reduced during TSR in sandstone was Cambrian to Ordovician seawater ($\delta^{34}S$ values of 27–33 ‰) diluted by subsurface formation waters which had oxidized pyrite in organic-rich shale of the Alum Shale Formation ($\delta^{34}S$ values of 14.5–16 ‰). A subordinate source of hydrogen sulfide for Pb-Zn sulfide ($\delta^{34}S$ values of 21–27 ‰ at Laisvall and 12–18 ‰ at Vassbo) was the replacement, at an early stage, of euhedral to subhedral pyrite and framboidal pyrite. A third localized source of hydrogen sulfide was identified at Laisvall in the feeder fault zone area of the Central Malm faults, where reduced sulfur fixed in sphalerite ($\delta^{34}S$ values of 2 ‰) was derived from sulfide (e.g., pyrrhotite, pyrite) in crystalline basement rocks.
- The Pb-Zn sulfide stage was locally accompanied by minor quartz dissolution. It is spatially associated with clusters of sphalerite-galena or with zones of barite dissolution. Quartz dissolution is interpreted to be triggered by

temperature increase or by organic acids and reactive cations (e.g., Ba^{2+} and K^{+}).

The proposed genetic model may be applied to explore for additional deposits in Sweden and Norway in autochthonous rocks along the erosional front or beneath the Caledonian orogen. Three key exploration tools are (i) the identification of reactivated basement structures, (ii) the identification and characterization (petrographic and geochemical) of pre-Pb-Zn sulfide stage barite cement, and (iii) the identification of the TSR process supplying H_2S for Pb-Zn sulfide precipitation.

Acknowledgments This research has been financially supported by Boliden AB (Sweden) and the Swiss National Science Foundation (SNF, Switzerland, FN 146 353). The Geological Survey of Sweden (SGU) provided financial and logistic support for much of the fieldwork in Sweden and for the participation of Michael B. Stephens. The staff members at SGU in Malå are thanked for their help at the national core archive. The authors are grateful to Boliden AB including Hans Årebäck (former exploration manager) and Rodney L. Allen (Manager Geology Research and Development) for financial and logistical support for the work carried out in Boliden and also for stimulating discussions. The staff working at the core archive in Boliden is acknowledged for supplying drill cores. Ulf Sandström, field technician in Boliden, is thanked for his help in managing the device during extraction of samples from outcrops in the Laisvall mine area. Dr. Thierry Adatte (University of Lausanne, Switzerland) is thanked for carrying out Rock-Eval and total organic carbon analyses of the shale samples. Stephen E. Kesler and Andrew Giże are thanked for their pertinent and detailed reviews. We would like to acknowledge the thorough review and editorial work by Karen D. Kelley.

References

Ader M, Sansjofre P, Halverson GP, Busigny V, Trindade RIF, Kunzmann M, Nogueira ACR (2014) Ocean redox structure across the Late Neoproterozoic Oxygenation Event: a nitrogen isotope perspective. Earth Planet Sci Lett 396:1–13

Anderson GM (2008) The mixing hypothesis and the origin of Mississippi Valley-type ore deposits. Econ Geol 103:1683–1690

Beaumont V, Robert F (1999) Nitrogen isotope ratios of kerogens in Precambrian cherts: record of the evolution of atmosphere chemistry? Precambrian Res 96:63–82

Ben Hassen A, Trichet J, Disnar J-R, Belayouni H (2010) Pétrographie et géochimie comparées des pellets phosphatés et de leur gangue dans le gisement phosphaté de Ras-Draâ (Tunisie). Implications sur la genèse des pellets phosphatés. Swiss J Geosci 103:457–473

Bennett PC (1991) Quartz dissolution in organic-rich aqueous systems. Geochim Cosmochim Acta 55:1781–1797

Bergman S, Stephens MB, Andersson J, Kathol B, Bergman T (2012) Geological map of Sweden: Geological Survey of Sweden, scale 1:1 000 000, 1 sheet

Bharati S, Patience RL, Larter SR, Standen G, Poplett IJF (1995) Elucidation of the Alum Shale kerogen structure using a multidisciplinary approach. Org Geochem 23:1043–1058

Bjørlykke A, Sangster DF (1981) An overview of sandstone lead deposits and their relation to red-bed copper and carbonate-hosted lead-zinc deposits. Econ Geol 75th Anniversary volume:179–213

Broman C (1983) Fluid inclusion thermometry in sphalerite from the Vassbo lead-zinc deposit, Sweden. Stockholm University, Ore Research Group, Annual Report, pp 103–116

Cao J, Hu K, Zhou J, Shi C, Bian L, Yao S (2013) Organic clots and their differential accumulation of Ni and Mo within early Cambrian black-shale-hosted polymetallic Ni-Mo deposits, Zunyi, South China. J Asian Earth Sci 62:531–536

Chowdhury AH, Noble JPA (1996) Origin, distribution and significance of carbonate cements in the Albert Formation reservoir sandstones, New Brunswick, Canada. Mar Pet Geol 13:837–846

Christofferson HC, Wallin B, Selkman S, Rickard DT (1979) Mineralization controls in the sandstone lead-zinc deposit at Vassbo, Sweden. Econ Geol 74:1239–1249

Claypool GE, Holser WT, Kaplan IR, Sakai H, Zak I (1980) The age curves of sulfur and oxygen isotopes in marine sulfate and their mutual interpretation. Chem Geol 28:199–260

Cremonese L, Shields-Zhou G, Struck U, Ling H-F, Och L, Chen X, Li D (2013) Marine biogeochemical cycling during the early Cambrian constrained by nitrogen and organic carbon isotope study of the Xiaotan section, South China. Precambrian Res 225:148–165

Dallmeyer RD, Gee DG (1986) $^{40}Ar/^{39}Ar$ mineral dates from retrogressed eclogites within the Baltoscandian miogeocline: implications for a polyphase Caledonian orogenic evolution. Geol Soc Am Bull 97:26–34

Dove PM (1999) The dissolution kinetics of quartz in aqueous mixed cation solutions. Geochim Cosmochim Acta 63:3715–3727

Dove PM, Nix CJ (1997) The influence of the alkaline earth cations, magnesium, calcium, and barium on the dissolution kinetics of quartz. Geochim Cosmochim Acta 61:3329–3340

Gee DG (1972) The regional geologic context of the Tåsjö uranium project, Caledonian front, Central Sweden. Geologic Survey of Sweden, Årsbok 66 2, Ser C, 671, 37

Gee DG (1975) A tectonic model for the central part of the Scandinavian Caledonides. Am J Sci 275A:468–515

Gee DG, Fossen H, Henriksen N, Higgins AK (2008) From the early Paleozoic platforms of Baltica and Laurentia to the Caledonide orogen of Scandinavia and Greenland. Episodes 31:1–8

Gee DG, Juhlin C, Pascal C, Robinson P (2010) Collisional orogeny in the Scandinavian Caledonides (COSC). J Geol Surv Sweden (GFF) 132:29–44

Gee DG, Ladenberger A, Dahlqvist P, Majka J, Be'eri-Shlevin Y, Frei D, Thomsen T (2013) The Baltoscandian margin detrital zircon signatures of the central Scandes. In: Corfu F, Gasser D, Chew DM (eds) New perspectives on the Caledonides of Scandinavia and related areas, vol 390. Geologic Society Special Publication, London, pp 131–155

Gelpi E, Schneider H, Mann J, Oro J (1970) Hydrocarbons of geochemical significance in microscopic algae. Phytochemistry 9:603–612

Gill BC, Lyons TW, Young SA, Kump LR, Knoll AH, Saltzman MR (2010) Geochemical evidence for widespread euxinia in the Later Cambrian ocean. Nature 469:80–83

Goldhaber MB, Orr WL (1995) Kinetic controls on thermochemical sulfate reduction as a source of sedimentary H_2S. In: Vairavamurthy MA, Schoonen MAA (eds) Geochemical transformations of sedimentary sulfur. ACS Symposium Series 612, pp 412–425

Greenwood PF, Brocks JJ, Grice K, Schwark L, Jaraula CMB, Dick JM, Evans KA (2013) Organic geochemistry and mineralogy. I. Characterization of organic matter associated with metal deposits. Ore Geol Rev 50:1–27

Greiling RO, Garfunkel Z (2007) An Early Ordovician (Finnmarkian?) foreland basin and related lithospheric flexure in the Scandinavian Caledonides. Am J Sci 307:527–553

Gromet LP, Sjöström H, Bergman S, Claesson S, Essex RM, Andreasson PG, Albrecht L (1996) Contrasts in ages of metamorphism in the Seve Nappes: U-Pb results from the central and northern Swedish Caledonides. J Geol Surv Sweden (GFF) 118:36–38

Hanor JS (1996) Controls on the solubilization of lead and zinc in basinal brines. Soc Econ Geol Spec Publ 4:483–500

Hanor JS (2000) Barite-celestite geochemistry and environments of formation. Rev Mineral Geochem 40:193–275

Heydari E, Moore CH (1989) Burial diagenesis and thermochemical sulfate reduction, Smackover Formation, southeastern Mississippi Salt Basin. Geology 12:1080–1084

Ishikawa T, Ueno Y, Komiya T, Sawaki Y, Han J, Shu D, Li Y, Maruyama S, Yoshida N (2008) Carbon isotope chemostratigraphy of a Precambrian/Cambrian boundary section in the Three Gorge area, South China: prominent global-scale isotope excursions just before the Cambrian Explosion. Gondwana Res 14:193–208

Israelson C, Halliday AN, Buchardt B (1996) U-Pb dating of calcite concretions from Cambrian black shales and the Phanerozoic time scale. Earth Planet Sci Lett 141:153–159

Johansson Å, Rickard DT (1984) Isotope composition of Phanerozoic ore leads from the Swedish Segment of the Fennoscandian Shield. Mineral Deposita 19:249–255

Kelley KD, Leach DL, Johnson CA, Clark JL, Fayek M, Slack JF, Anderson VM, Ayuso RA, Ridley WI (2004) Textural, compositional, and sulfur isotope variations of sulfide minerals in the Red Dog Zn-Pb-Ag deposits, Brooks Range, Alaska: implications for ore formation. Econ Geol 99:1509–1532

Kendrick MA, Burgess R, Harrison D, Bjørlykke A (2005) Noble gas and halogen evidence for the origin of Scandinavian sandstone-hosted Pb-Zn deposits. Geochim Cosmochim Acta 69:109–129

Knauss KG, Copenhaver SA, Braun RL, Burnham AK (1997) Hydrous pyrolysis of New Albany and Phosphoria Shales: production kinetics of carboxylic acids and light hydrocarbons and interactions between the inorganic and organic chemical systems. Org Geochem 27:477–496

Krahn L, Baumann A (1996) Lead isotope systematics of epigenetic lead-zinc mineralization in the western part of the Rheinisches Schiefergebirge, Germany. Mineral Deposita 31:225–237

Kribek B, Zak K, Spangenberg JE, Jehlicka J, Prokes S, Kominek J (1999) Bitumens in the late Variscan hydrothermal vein-type uranium deposit of Pribram, Czech Republic; sources, radiation-induced alteration, and relation to mineralization. Econ Geol 94(7):1093–1114

Kribek B, Sykorova I, Pasava J, Machovic V (2007) Organic geochemistry and petrology of barren and Mo-Ni-PGE mineralized marine black shales of the Lower Cambrian Niutitang Formation (South China). Coal Geol 72:240–256

Krouse HR, Viau CA, Eliuk LS, Ueda A, Halas S (1988) Chemical and isotopic evidence of thermochemical sulfate reduction by light hydrocarbon gases in deep carbonate reservoirs. Nature 333:415–419

Kullerud K, Stephens MB, Zachrisson E (1990) Pillow lavas as protoliths for eclogites: evidence from a late Precambrian–Cambrian continental margin Seve Nappes, Scandinavian Caledonides. Contrib Mineral Petrol 99:344–351

Leach DL, Sangster DF, Kelley KD, Large RR, Garven G, Allen CR, Gutzmer J, Walters S (2005) Sediment-hosted Pb-Zn deposits: a global perspective. Economic Geology 100th Anniversary volume: 561–607

Lindblom S (1986) Textural and fluid inclusion evidence for ore deposition in the Pb-Zn deposit at Laisvall, Sweden. Econ Geol 81:46–64

Ljungner E (1950) Urbergsytans form vid Fjällranden. J Geol Surv Sweden (GFF) Bd 72:H 3 (in Swedish)

Lucks TJ (2004) Controls on the ore distribution of the Laisvall deposit, Sweden. Unpublished doctoral thesis, University of Cardiff, Cardiff, UK

Machel HG (1987) Some aspects of diagenetic sulfate-hydrocarbon redox-reactions. In: Marshall JD (ed) Diagenesis of sedimentary sequences. Geol Soc Spec Publ 36:15–28

Machel HG (2001) Bacterial and thermochemical sulfate reduction in diagenetic settings—old and new insights. Sediment Geol 140: 143–175

Menotti TA (2006) Lower Paleozoic oxygen isotope values from carbonate rocks: primary or diagenetic? Senior thesis in geosciences, Bachelor of Science, Pennsylvania State University, Pennsylvania, USA, pp 43

Muhling JR, Fletcher IR, Rasmussen B (2012) Dating fluid flow and Mississippi Valley-type base-metal mineralization in the Paleoproterozoic Earaheedy Basin, Western Australia. Precambrian Res 212–213:75–90

Nelson GJ, Pufahl PK, Hiatt EE (2010) Paleoceanographic constraints on Precambrian phosphorite accumulation, Baraga Group, Michigan, USA. Sediment Geol 226:9–21

Nielsen AT, Schovsbo NH (2011) The Lower Cambrian of Scandinavia: depositional environment, sequence stratigraphy and paleogeography. Earth Sci Rev 107:207–310

Ohmoto H, Rye RO (1979) Isotopes of sulfur and carbon. In: Barnes HL (ed) Geochemistry of hydrothermal ore deposits. Wiley, New York, pp 509–567

Prokoph A, Shields GA, Veizer J (2008) Compilation and time-series analysis of a marine carbonate $\delta^{18}O$, $\delta^{13}C$, $^{87}Sr/^{86}Sr$ and $\delta^{34}S$ database through Earth history. Earth Sci Rev 87:113–133

Rasmussen B (1996) Early diagenetic REE-phosphate minerals (florencite, gorceixite, crandallite, and xenotime) in marine sandstones: a major sink for oceanic phosphorous. Am J Sci 296:601–632

Rickard DT (1983) Precipitation and mixing mechanisms in Laisvall-type sandstone Pb-Zn deposits. In: Kirsvarsanyi G, Hagni R, Pratt W, Koening JW (eds) Proceedings of the International Conference on Mississippi Valley Type Lead-Zinc Deposits. Rolla, Missouri

Rickard DT, Willdén M, Mårde Y, Ryhage R (1975) Hydrocarbons associated with Pb–Zn ores at Laisvall, Sweden. Nature 255:131–133

Rickard DT, Willdén MY, Marinder NE, Donnelly TH (1979) Studies on the genesis of the Laisvall sandstone lead-zinc deposit, Sweden. Econ Geol 74:1255–1285

Rickard DT, Coleman M, Swainbank I (1981) Lead and sulfur isotopic compositions of galena from the Laisvall sandstone Pb-Zn deposit, Sweden. Econ Geol 76:2042–2046

Rimstidt JD (1977) Gangue mineral transport and deposition. In: Barnes HL (ed) Geochemistry of hydrothermal ore deposits, 3rd edn. Wiley, New York, pp 487–515

Roberts D, Gee DG (1985) An introduction to the structure of the Scandinavian Caledonides. In: Gee DG, Sturt BA (eds) The Caledonide Orogen–Scandinavia and related areas. Wiley, Chichester, pp 55–68

Roberts D, Siedlecka A (2002) Timanian orogenic deformation along the northeastern margin of Baltica, Northwest Russia and Northeast Norway, and Avalonian–Cadomian connections. Tectonophysics 352:169–184

Romer R (1992) Sandstone-hosted lead-zinc mineral deposits and their relation to the tectonic mobilization of the Baltic Shield during the Caledonian orogeny, a reinterpretation. Miner Petro 47:67–85

Root D, Corfu F (2012) U-Pb geochronology of two discrete Ordovician high-pressure metamorphic events in the Seve Nappe Complex Scandinavian Caledonides. Contrib Mineral Petrol 163:769–788

Saintilan NJ (2015) Key controls, age, source of metals and role of hydrocarbons on the origin of Laisvall-type Pb-Zn deposits and their relationship to calcite-fluorite-Zn ± Pb sulfide vein-type mineralization in Baltica basement (Sweden). PhD thesis, University of Geneva, Geneva, Switzerland, pp 235

Saintilan NJ, Stephens MB, Lundstam E, Fontboté L (2015a) Control of reactivated basement structures on sandstone-hosted Pb-Zn deposits along the Caledonian Front, Sweden: evidence from airborne magnetic field data, structural analysis and ore grade modeling. Econ Geol 110:91–117

Saintilan NJ, Schneider J, Stephens MB, Chiaradia M, Kouzmanov K, Wälle M, Fontboté L (2015b) A Middle Ordovician age for the Laisvall sandstone-hosted Pb-Zn deposit, Sweden: a response to early Caledonian orogenic activity. Econ Geol 110:1779–1801

Santallier DS (1988) Mineralogy and crystallization of the Seve eclogites in the Vuoggatjålme area. Swedish Caledonides of Norrbotten. J Geol Soc Sweden (GFF) 110:89–98

Shen C, Pratt BR, Zhang X-G (2014) Phosphatized coprolites from the middle Cambrian (stage 5) Duyun fauna of China. Palaeogeogr Palaeoclimatol Palaeoecol 410:104–112

Shields-Zhou G, Zhu M (2013) Biogeochemical changes across the Ediacaran–Cambrian transition in South China. Precambrian Res 225:1–6

Simpson G, Yang C, Hutcheon I (1996) Thermochemical sulfate reduction: a local process that does not generate thermal anomalies. In: Ross GM (ed) Alberta Basement Transect Workshop, Lithoprobe Report 51, pp 241–245

Skiöld T (1988) Implications of new U-Pb zircon chronology to early Proterozoic crustal accretion in northern Sweden. Precambrian Res 38:147–164

Söderlund U, Isachsen C, Bylund G, Heaman L, Patchett PJ, Vervoort JD, Andersson UB (2005) U-Pb baddeleyite ages and Hf, Nd isotope chemistry constraining repeated mafic magmatism in the Fennoscandian Shield from 1.6 to 0.9 Ga. Contrib Mineral Petrol 150:174–194

Soudry D, Champetier Y (1983) Microbial processes in the Negev phosphorites (southern Israel). Sedimentology 30:411–423

Spangenberg JE, Frimmel HE (2001) Basin-internal deviation of hydrocarbons in the Witwatersrand Basin, South Africa: evidence from bulk and molecular $\delta^{13}C$ data. Chem Geol 173:339–355

Spangenberg JE, Herlec U (2006) Hydrocarbon biomarkers in the Topla-Mežica Zn-Pb deposits, Northern Karavanke/Drau Range, Slovenia: paleoenvironment at the site of ore formation. Econ Geol 101:997–1021

Spangenberg JE, Macko SA (1998) Organic geochemistry of the San Vicente Zn-Pb district, eastern Pucará Basin, Peru. Chem Geol 146:1–23

Spangenberg JE, Bagnoud-Velásquez M, Boggiani PC, Gaucher C (2014) Redox variations and bioproductivity in the Ediacaran: evidence from inorganic and organic geochemistry of the Corumbá Group, Brazil. Gondwana Res 26:1186–1207

Stephens MB (1988) The Scandinavian Caledonides: a complexity of collisions. Geol Today 4:20–26

Sturt BA (1978) The Norwegian Caledonides. Geol Surv Can Pap 78:13–16

Surdam RC, Yin P (1993) Organic acids and carbonate stability, the key to predicting positive porosity anomalies. In: Pittman ED, Lewan MD (eds) Organic acids in geological processes. Springer, Berlin, pp 399–448

Surdam RC, Boese SW, Crossey LJ (1984) The chemistry of secondary porosity. In: McDonald DA, Surdam RC (eds) Clastic diagenesis, American Association of Petroleum Geologists Memoir 37, pp 127–149

Thickpenny A (1984) The sedimentology of the Swedish alum shales. In: Stow DAV, Piper DJW (eds) Fine-grained sediments, Geological Society Special Publications 15, London, pp. 511–525

Thom J, Anderson GM (2008) The role of thermochemical sulfate reduction in the origin of Mississippi Valley-type deposits. I. Experimental results. Geofluids 8:16–26

Veizer J (2004) Isotope data, Phanerozoic database, $\delta^{18}O$ update-2004: http://www.science.uottawa.ca/geology/isotope_data

Veizer J, Ala D, Azmy K, Bruckschen P, Buhl D, Bruhn F, Carden GAF, Diener A, Ebneth S, Godderis Y, Jasper T, Korte C, Pawellek F, Podlaha OG, Strauss H (1999) $^{87}Sr/^{86}Sr$, $\delta^{13}C$ and $\delta^{18}O$ evolution of Phanerozoic seawater. Chem Geol 161:59–88

Vidal G, Nystuen JP (1990) Lower Cambrian acritarchs and the Proterozoic–Cambrian boundary in southern Norway. Nor Geol Tidsskr 70:191–222

Wallin B (1982) Sedimentology of the Lower Cambrian sequence at Vassbo, Sweden. PhD thesis, Acta Universitatis Stockholmiensis, Stockholm, Sweden

Willdén MY (1980) Paleoenvironment of the autochthonous sedimentary rocks sequence at Laisvall, Swedish Caledonides. PhD thesis, Stockholms Universitets Geologiska Institutionen, Stockholm, Sweden

Worden RH, Smalley PC, Oxtoby NH (1995) Gas souring by thermochemical sulfate reduction at 140°C. Am Assoc Pet Geol Bull 79: 854–863

Xue C, Zeng R, Liu S, Chi G, Qing H, Chen Y, Yang J, Wang D (2007) Geologic, fluid inclusion and isotopic characteristics of the Jinding Zn–Pb deposit, western Yunnan, South China: a review. Ore Geol Rev 31:337–359